Control of isolated response curves through optimization of codimension-1 singularities

Adrien Mélot, Enora Denimal, Ludovic Renson

Control of isolated response curves through optimization of codimension-1 singularities

Adrien Mélot[a,*], Enora Denimal Goy[b] and Ludovic Renson[c]

[a]Univ. Gustave Eiffel, Inria, COSYS-SII, I4S, Campus Beaulieu, Rennes, France
[b]Inria, CMAP, Ecole Polytechnique, IPP, Palaiseau, France
[c]Dynamics Group, Department of Mechanical Engineering, Imperial College London, London, United Kingdom

ARTICLE INFO

Keywords:
Harmonic balance method
Nonlinear vibrations
Bifurcation tracking
Singularity
Stability
Isola

ABSTRACT

We introduce a computational framework for controlling the location of isolated response curves, i.e. responses that are not connected to the main solution curve and form a closed curve in parameter space. The methodology relies on bifurcation tracking to follow the evolution of fold bifurcations in a codimension-2 parameter space. Singularity theory is used to distinguish points of isola formation and merger from codimension-2 bifurcations and an optimization problem is formulated to delay or advance the onset or merger of isolated response curves or control their position in the state/parameter space. We illustrate the methodology on three examples: a finite element model of a cantilever beam with cubic nonlinearity at its tip, a two-degree-of-freedom oscillator with asymmetry and a two-degree-of-freedom base-excited oscillator exhibiting multiple isolas. Our results show that the location of points of isola formation and mergers can effectively be controlled through structural optimization.

1. Introduction

Numerical continuation is a commonly employed tool to study the behaviour of nonlinear systems as parameters are varied.In mechanical engineering, one of those parameters is often the excitation frequency. This allows for tracing out the so-called forced (or frequency) response curves (FRCs), i.e. one-dimensional submanifolds of solutions connected to each other under continuous variation of the excitation frequency. The FRCs of the beam structure considered in this study are illustrated in Fig. 1 (solid blue) for three different values of forcing amplitude. Classical continuation approaches are initialised based on an estimation of the solution at low energies, i.e. where the solution can be satisfactorily approximated using linear techniques.

Isolated response curves (IRCs), also known as detached response curves or isolas, are branches of solutions which form closed curves in the parameter space, as illustrated with the FRCs computed at $F = 75$ N in Fig. 1. They are not connected to the main solution branch, i.e. the branch continued from the quasi-linear solutions and, consequently, are often overlooked during continuation analyses. Nonetheless, they can merge with the main branch when a parameter such as the forcing amplitude is varied, or even merge with another isola, resulting in a *superisola* [39, 40]. The presence of isolas have been reported in numerous numerical and experimental studies, with the first reports dating back to the 1950s [1]. They can be found in nonlinear mechanical systems affected by various nonlinearities: polynomial [69, 50, 64, 30], contact and friction [66, 29, 40, 76, 67, 77], hysteretic and piecewise linear elastic restoring forces [10, 23, 2, 28], hertzian contact [62]. They were also uncovered in traffic flow [53], flight dynamics models [59] and systems controlled with rate-limited feedback [58]. Other fields include chemical engineering [12, 47, 24] and laser physics [20]. For a more in-depth review, we refer the interested reader to [38].

If undetected, isolas can be dangerous for they can lead to multi-stable regions with high amplitude responses where a single low amplitude response would otherwise be expected [3]. They can also induce substantial increases in amplitude as well as frequency shifts when the merger with the main solution branch occurs on the primary resonance, as shown in Fig. 1. They can also prove useful. For instance, IRCs created by imperfect pitchforks induced by symmetry breaking may be exploited for infinitesimal mass detection [37]. Their detection and computation are, therefore, of primary interest. A number of authors proposed analytical techniques to predict and compute isolas [42, 39, 63]. Salles *et al.* [66] proposed a method for computing the whole FRCs including IRCs induced by imperfect bifurcations. Their method relies on the computation of the tangents of the emanating branches at the imperfect bifurcation point to switch to the IRC. However, this method only works for IRCs that are close to the main branch. An alternative is deflated continuation [26, 25] which, contrary to common predictor/corrector-based continuation algorithms, allows one to compute detached solution branches by penalizing a solution found from a given initial guess so that the solver converges to another. Nevertheless, this induces a higher computational burden and potential convergence issues. The most widespread numerical technique for studying IRCs in mechanical engineering is arguably bifurcation tracking, which consists in following the location of a bifurcation point in a codimension-2 parameter space. IRCs being closed curves, they exhibit at least two fold bifurcations[1]. It is, therefore, possible to

*Corresponding author
adrien.melot@inria.fr (A. Mélot)
ORCID(s): 0000-0002-7939-5548 (A. Mélot)

[1]Throughout this paper, the terms limit point, turning point and fold point will be used interchangeably.

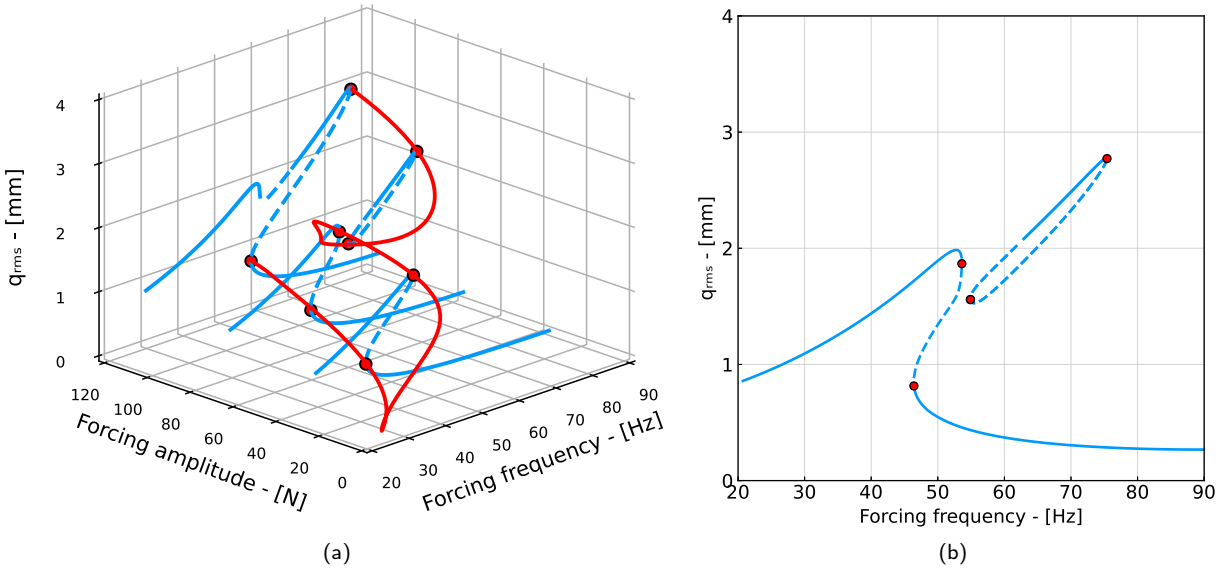

Figure 1: Example of FRCs and fold bifurcation tracking curve of a cantilever beam (a) and projection in the amplitude-frequency plane of the FRCs at a forcing amplitude equal to 75 N (b). Stable and unstable solutions are represented by solid (—) and dashed (- - -) lines, respectively. Fold bifurcations are denoted by red (●) circle markers.

follow a fold with respect to the excitation frequency and another parameter, e.g. the forcing amplitude, and detect an isola when the fold curve exhibits multiple solutions for a given value of the tracking parameter (Fig. 1). The first attempts at studying IRCs through fold bifurcation tracking are not recent [14, 44, 45]. More recently Detroux *et al.* [19] used it to reveal the existence of an IRC and its merger in the frequency response of a satellite structure. Kuether *et al.* [50] developed a method based on nonlinear normal modes and energy balance to detect IRCs and employed bifurcation tracking to study the IRC associated with a 3:1 internal resonance of a cantilever beam with cubic nonlinearity.

In this paper, we introduce a computational methodology to optimize the design of engineered systems in order to control the location of isolas in the parameter space. Recent works have developed optimization methods to control bifurcations [8, 7, 55] or identify the system parameters leading a specific bifurcation diagram [73]. Pedersen [60] optimized the topology of a plate to suppress internal resonances. Dou *et al.* [21, 22] optimized the non-uniform width of structural elements to attenuate the amplitude of nonlinear resonances of a beam and to modify the hardening/softening behaviour of planar structures. Detroux *et al.* [17] optimized the form of the nonlinearity to optimize the shape of the backbone curves of nonlinear systems in order to suppress modal interactions and enforce isochronicity. More recently, Denimal *et al.* [15, 16] mitigated vibrations in bladed disks by optimizing the topology of under-platform dampers to maximize energy dissipation.

We introduce herein an optimization strategy which relies on a series of continuation analyses in codimension-2 to compute curves of fold bifurcations. The methodology is general in that it does not depend on the technique used to discretize the periodic solutions (harmonic balance, collocation, etc). The fundamental assumption of the methodology is that *a priori* knowledge regarding the parameters governing the isola formation and merger as well as the bifurcation involved is available. Although the computational foundations to carry out bifurcation tracking are relatively well established [19, 78, 2, 56], adapting it to be suitable for an optimization procedure is challenging and requires the systematic detection and classification of the turning points along the bifurcation tracking curves into isola formation and merger points. This is one of the novelties of this work. In particular, we propose herein several test functions that allow one to detect and classify such points in a way that is compatible with an optimization procedure. Turning points of the fold curves are detected and points of isola formation and merger, i.e. codimension-1 singularities, are identified and discriminated from codimension-2 bifurcations using singularity theory.

Few authors have attempted to account for IRCs into system design in the past and the formulation of a multi-parametric or shape optimization problem to directly control the location of isolas has never been formally attempted. Kernevez *et al.* [48] employed continuation to follow the location of isola formation points in a biochemical system with perturbed bifurcations with respect to a single design parameter. In [36], Grenat *et al.* developed a multi-parametric recursive continuation analysis method to identify the set of parameters of a nonlinear tuned vibration absorber which best delays the birth of an isola or minimizes the distance between birth and merger. However, their method relies on successive continuation analyses with an increased number of parameters

at each step of the algorithm, which can lead to intractable computations for high-dimensional systems. Additionally, it is unclear how the methodology behaves when the system exhibits multiple isolas. More recently, Nguyen *et al.* [59] used bifurcation tracking to identify the minimum controller gain to apply to suppress the IRC in a flight dynamics model. Our methodology differs in that it is able to handle multi-parametric optimizations with hundreds of parameters and even shape optimizations while relying only on successive codimension-2 bifurcation tracking analyses.

The paper is structured as follows. In section 2, we formulate the optimization problem used to control isolated response curves, introduce the principles of continuation in codimension-2 and the main theoretical results needed to characterize points of isola formation and merger. We emphasize the fact that the computational methods employed hereafter are chosen for their good performance when solving mechanical problems. Nonetheless, other methods could be considered depending on the problem at hand. The capabilities of the developed methodology are illustrated in Sect. 3 and Sect. 4 concludes the paper.

2. Formulation of the optimization problem

We formulate here a general optimization problem whose purpose is to determine a set of design parameters for controlling the location of isolated response curves in the parameter space. The evaluation of the objective functional is based on successive codimension-2 continuation analyses, i.e. bifurcation tracking analyses, of fold bifurcation points which belong to the IRCs. The points of isola formation and merger are then identified on the computed curves using criteria on the local topology of the solution manifold near those points.

We consider general optimization problems of the form:

$$\begin{aligned} &\underset{\boldsymbol{\theta}}{\text{maximize}} \quad \mathcal{F} \\ &\text{subject to} \quad b_i^l \leq \theta_i \leq b_i^u \qquad \forall i \in [\![1, p]\!], \end{aligned} \tag{1}$$

where $\mathcal{F}$ is the considered objective functional, $\boldsymbol{\theta} \in \mathbb{R}^p$ is the vector of optimization (design) variables. We consider hereafter only simple box constraints defined with vectors $\mathbf{b}^l$ and $\mathbf{b}^u$ to ensure that the design parameters assume realistic values. However, the consideration of more complicated constraints is straightforward, provided the chosen optimization algorithm is capable of handling them.

2.1. Definition of the objective functional

Several objectives can be defined regarding the location of IRCs in the parameter space. We herein understand the term location as the value of an operating parameter μ whose variation may lead to the formation and merger of an IRC, an example being the amplitude of the external forcing, as illustrated in Fig. 2. In the following, we formulate several problems that can have particular relevance in many engineering applications. Let us denote by $(q_{\text{birth}}, \mu_{\text{birth}})$ and $(q_{\text{merger}}, \mu_{\text{merger}})$ the amplitude and parameter values at which the IRC is created (red diamond marker (◆) in Fig. 2) and merges (orange diamond marker (◆) in Fig. 2) with the main solution branch, respectively. These values are computed via bifurcation tracking as detailed in the next section.

Problem 1: delay the onset of isola. The most straightforward objective is to delay the appearance of the point of isola formation in order to increase the range of parameter without multi-stability, i.e. shifting the red diamond marker (◆) towards higher forcing amplitudes in Fig. 2. Suppose the onset and merger of the IRC occur for increasing values of parameter μ. The objective functional can be expressed as:

$$\underset{\boldsymbol{\theta}}{\text{maximize}} \quad \mathcal{F} = \mu_{\text{birth}} \tag{2}$$

Problem 2: delay the isola merger. One may also want to delay the merger (shifting the orange diamond marker (◆) towards higher forcing amplitudes in Fig. 2) in order to delay the dramatic amplitude and frequency shifts generated by the merger with the primary resonance. In this case, the objective function would be expressed as:

$$\underset{\boldsymbol{\theta}}{\text{maximize}} \quad \mathcal{F} = \mu_{\text{merger}} \tag{3}$$

Problem 3: shift the onset of isola to a target location. Suppose one wants to enforce the appearance of a point of isola formation and/or merger at a specific location. Taking a point of isola formation as an example, the objective functional would read:

$$\underset{\boldsymbol{\theta}}{\text{minimize}} \quad \mathcal{F} = \left| \frac{\mu_{\text{birth}} - \mu_{\text{target}}}{\mu_{\text{target}}} \right| \tag{4}$$

Problem 4: set a target amplitude for the point of isola formation. As a final example, we consider cases where the point of isola formation cannot be pushed sufficiently far away from the expected maximum forcing amplitude. In this case, one could want to enforce the amplitude of the point of isola formation, e.g. placing it below the main solution branch to mitigate the risk of high amplitude vibrations in the multi-stable zone:

$$\underset{\boldsymbol{\theta}}{\text{minimize}} \quad \mathcal{F} = \left| \frac{q_{\text{birth}} - q_{\text{target}}}{q_{\text{target}}} \right| \tag{5}$$

Note that several objectives may also be considered, via either multi-objective optimization or regularisation techniques with weighted sums [52], depending on the target application and relative position of the IRC with respect to the main solution branch, e.g. to control the location of both the formation and merger points, to delay the birth of an IRC and place it at a targeted amplitude or frequency or to simultaneously control an IRC and bifurcations occurring on the main branch similarly to what was introduced in [55], or even minimize the curvature at the point of isola formation in order to control its growth rate. Although such cases are not considered in this paper, the required information can be readily retrieved in the output of the bifurcation tracking analysis presented in the following section.

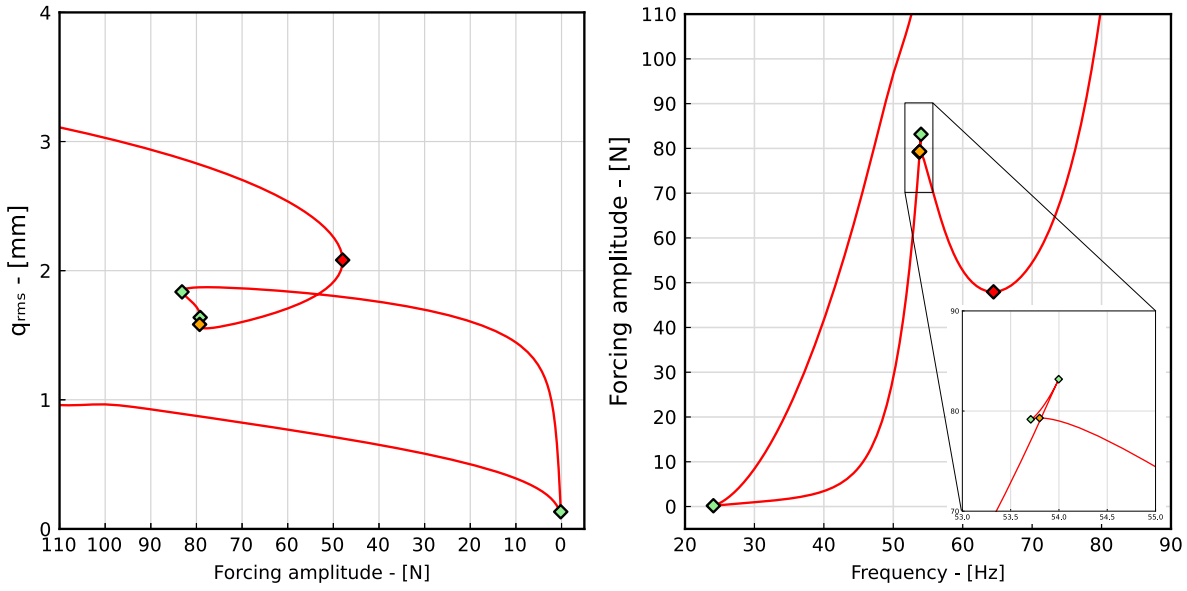

Figure 2: Projections in the amplitude-forcing amplitude (a) and forcing amplitude-frequency (b) planes of the fold bifurcation tracking curve shown in Fig. 1. The fold bifurcation curve is shown as a solid red line. Green (◆), red (◆) and orange (◆) diamond markers represent cusp bifurcations and points of isola formation and merger, respectively.

2.2. Continuation in codimension-2

Without loss of generality, we herein resort to the harmonic balance method (HBM) [75, 49], which consists in enforcing the periodicity of the sought solutions with Fourier series expansions, in order to transform the equations of motion into a system of nonlinear algebraic equations that can be solved with a continuation algorithm:

$$\boldsymbol{\mathcal{R}}(\boldsymbol{\theta} = \mathbf{cst}, \mathbf{q}, \eta, \mu) = \boldsymbol{\mathcal{R}}(\mathbf{q}, \eta, \mu) = \mathbf{0} \tag{6}$$

where $\boldsymbol{\theta} \in \mathbb{R}^p$ is the vector of design parameters, which only changes between two optimization iterations. Vector $\mathbf{q} \in \mathbb{R}^n$ is the system's discretised states and $(\eta, \mu) \in \mathbb{R}^2$ are a bifurcation and an auxiliary parameters, respectively.

Solutions to this zero problem form a two-dimensional solution manifold shown in light grey in Fig. 3. Fixing η and μ allows one to compute points on this manifold by solving the following system:

$$\boldsymbol{\mathcal{R}}(\boldsymbol{\theta} = \mathbf{cst}, \mathbf{q}, \eta = cst, \mu = cst) = \mathbf{0}. \tag{7}$$

However, it is usual to allow parameter η to vary to trace out codimension-1 curves, i.e. one-dimensional submanifolds of (6) (the blue and purple curves in Fig. 1 and Fig. 3, respectively), with a continuation technique. Such curves would correspond to FRCs should the variable parameter η be chosen as the excitation frequency Ω. Since the solution algorithm has to be able to compute turning points, we parameterize the one-dimensional solution submanifold by its arc-length s [68] so that $\mathbf{q} = \mathbf{q}(s)$ and $\eta = \eta(s)$ and treat parameter η as an additional unknown:

$$\mathbf{R}(\boldsymbol{\theta} = \mathbf{cst}, \mathbf{q}, \eta, \mu = cst) = \begin{pmatrix} \boldsymbol{\mathcal{R}}(\mathbf{q}, \eta) \\ p(\mathbf{q}, \eta) \end{pmatrix} = \mathbf{0}. \tag{8}$$

where $\mathbf{R}$ is formed by appending the arclength equation $p(\mathbf{q}, \eta)$ to $\boldsymbol{\mathcal{R}}$, which constrains the sought solution to lie at the intersection of the solution branch and a hypersphere of radius Δs corresponding to the current step size of the continuation algorithm:

$$p(\mathbf{q}, \eta, s) = (\Delta\mathbf{q})^T (\Delta\mathbf{q}) + \Delta\eta^2 - \Delta s^2 = 0. \tag{9}$$

where $\Delta\mathbf{q}$, $\Delta\eta$ are the components of the tangent vector $\Delta\mathbf{Q} = (\Delta\mathbf{q}, \Delta\eta)^T$ at the previous solution point, which also serves to provide an initial guess to the solver at each continuation iteration.

Bifurcations on this curve occur when the Jacobian becomes singular:

$$\det \partial_{\mathbf{q}} \boldsymbol{\mathcal{R}}(\boldsymbol{\theta} = \mathbf{cst}, \mathbf{q}, \eta, \mu = cst) = \mathbf{0} \tag{10}$$

and can be detected and classified using dedicated stability and bifurcation analysis techniques [51, 6]. The evolution of bifurcation points can, in turn, be followed with respect to an additional parameter μ, hereafter referred to as bifurcation tracking parameter. This corresponds to a continuation analysis in a codimension-2 parameter space (red curves in both Fig. 2 and Fig. 3). Consequently, due to the additional unknown, another equation has to be appended to system (8) to provide closure:

$$\mathbf{R}(\mathbf{q}, \eta, \mu) = \begin{pmatrix} \boldsymbol{\mathcal{R}}(\mathbf{q}, \eta, \mu) \\ p(\mathbf{q}, \eta, \mu) \\ g(\mathbf{q}, \eta, \mu) \end{pmatrix} = \mathbf{0}. \tag{11}$$

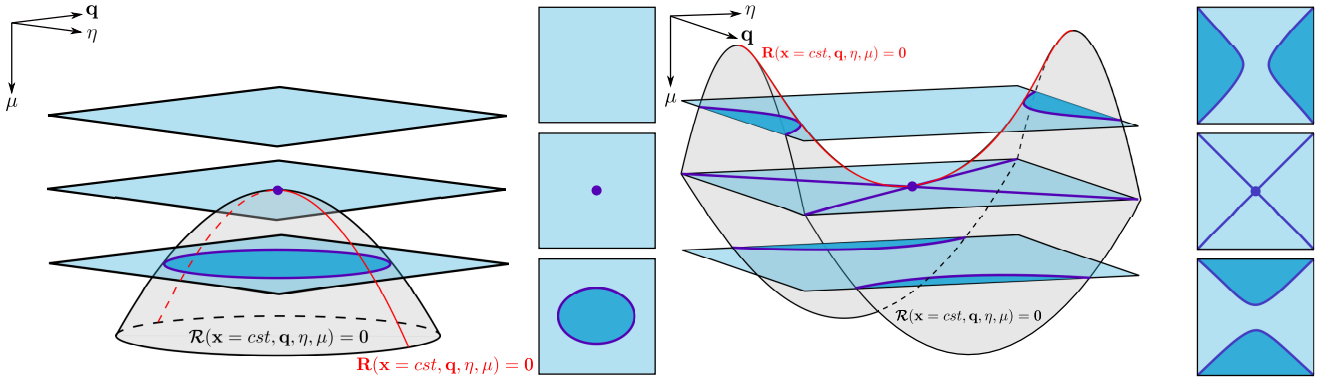

(a) (b)

Figure 3: Illustration of elliptic turning point leading to isola formation (a) and hyperbolic turning point leading to isola merger (b). The local topology of the solution manifold is shown in light grey. Blue surfaces are planes where μ is constant. Purple and red lines are frequency response curves solutions to Eq. (8) and fold tracking curves solutions to Eq. (11), respectively.

Function $g(\mathbf{q}, \eta, \mu)$ is a bifurcation-constraining function which equals zero when the solution point is a specific bifurcation. It is here limited to a scalar function as our method is based on minimally extended systems [33, 19, 56, 57]. However one could also use standard extended systems [54, 78]. It is evaluated via the solution of a bordered linear system [4, 35] which, for fold bifurcations, takes the following form:

$$\begin{bmatrix} \partial_{\mathbf{q}}\boldsymbol{\mathcal{R}} & \mathbf{b} \\ \mathbf{d}^{\dagger} & 0 \end{bmatrix} \begin{pmatrix} \mathbf{w} \\ g \end{pmatrix} = \begin{pmatrix} \mathbf{0} \\ 1 \end{pmatrix} \tag{12}$$

where $\mathbf{b}$ and $\mathbf{d}$ are chosen to ensure the non-singularity of the system [34].

2.3. Practical considerations

Bifurcation tracking computes the evolution of characteristic points, here fold bifurcations, in a given parameter interval. The bifurcation tracking parameter μ ought to be chosen for its leveraging effects on isola creation and merger with additional solution branches. Since we want to control the location of IRCs, we assume that *a priori* knowledge of the system is available and that the key parameters are already identified. If no a priori knowledge is available, a global search method similar to the one introduced in [40] could be investigated to detect isolas and coupled to bifurcation tracking to determine influential parameters.

As with all continuation algorithms, a starting point has to be provided to the solver. For fold bifurcation tracking, an initial point can be found by performing an initial continuation in codimension-1 with μ kept fixed. For the examples considered here, η corresponds to the angular frequency Ω. Turning points along this curve can be identified by monitoring the η-component of the tangent vector $\Delta\eta$ and then used to initiate the codimension-2 continuation. For simplicity, we use the fold bifurcation located at the top of the merged isola as a starting point. This obviously requires the isola to be merged with the primary resonance which is not guaranteed during iterations of the optimization solver. Additionally, during optimization, the design parameters are expected to change, which could lead to points of interest, e.g. points of isola formation, lying outside of the considered interval of parameter η. A solution could consist in computing the fold curve in a large enough interval. However, this can prove costly and even lead to intractable computations for large-scale systems. In this work, we circumvent this issue by adapting the tracking interval during optimization iterations. If, at a given iteration, the isola has not merged with the main solution branch, we increase the size of the tracking interval and run another FRC computation with the updated

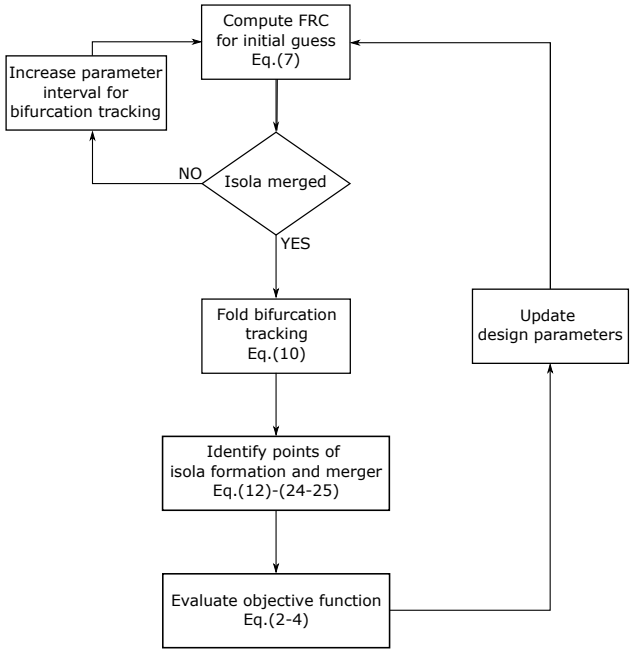

Figure 4: Flowchart of the computation of the optimization methodology.

extremum value of the tracking parameter (Fig. 4). This requires finding a trade-off between the added cost of computing additional FRCs and increasing the size of the tracking interval, resulting in more solution points being computed. However, the increase in computational effort is relatively minor since additional FRCs are only computed when absolutely necessary and the modifications to the optimization variables are expected to have a similar qualitative influence on both points of isola formation and merger.

2.4. Detection and classification of codimension-1 singularities

Solving Eq. (11) in a given parameter interval yields a fold curve, i.e. regular points of Eq. (11) corresponding to fold bifurcations of Eq. (8) for different fixed values of μ. This curve can itself exhibit bifurcations [65, 27]. Since they require the variation of two parameters to occur, we refer to these as codimension-2 bifurcations. Following standard practices in bifurcation analysis, we define test functions whose zeros indicate a specific bifurcation. Utilizing test functions allows for a systematic and automated detection and classification of the points along the bifurcation tracking, making it compatible with an optimization procedure.

Turning points of the fold curve are easily identified by monitoring the sign of the μ-component of the tangent vector:

$$\varphi_F = \Delta\mu \tag{13}$$

The above test function does not discriminate between cusp bifurcations and points of isola formation and merger. Thus, additional conditions must be derived to distinguish them.

Singularity theory allows one to study how bifurcation diagrams behave qualitatively under perturbations and to classify equivalent regions of the solution manifold where bifurcation points are seen as organizing centres of the local dynamics. Within the framework of singularity theory, parameter μ is seen as a *perturbation or unfolding parameter* instead of an auxiliary parameter. Several works addressed the link between bifurcation curves and singularities [13, 70, 45, 68, 11, 39]. Singularities of a given codimension act as organizing centers for singularities of lower codimension. In particular, codimension-1 singularities give birth to codimension-0 singularities, i.e. codimension-1 fold bifurcations and, in the special case of a system exhibiting Z_2-symmetry, pitchforks. Thus, codimension-1 singularities of Eq. (6) are turning points of the fold curve [70, 45] and the bifurcation tracking can be seen as a codimension-0 singularity tracking.

We present here fundamental results from singularity theory that allow one to characterize isolated response curves. Consider the following scalar equation:

$$h(u, \eta, \mu) = 0 \tag{14}$$

where $u \in \mathbb{R}$. A specific point on the solution manifold corresponds to a singularity, i.e. a boundary between two non-equivalent bifurcation diagrams, if a number of conditions are met. These can be split into two groups: defining and non-degeneracy conditions. All singularities are characterized by the following defining conditions:

$$h = 0, \quad \partial_u h = 0 \tag{15}$$

Since we restrict ourselves to bifurcation diagrams defined by equations like (6) with only one unfolding parameter, we limit this section to a discussion on codimension-1 singularities, of which there exist three types: *hysteresis*, *isola* and *simple bifurcation*.

Hysteresis singularities. Hysteresis singularities are defined by the following non-degeneracy conditions:

$$\partial_\eta h \neq 0, \quad \partial_{uu} h = 0, \quad \partial_{uuu} h = 0 \tag{16}$$

where $\partial_{uu} h$ and $\partial_{uuu} h$ denote double and triple differentiation with respect to u, respectively.

Isola singularities. The non-degeneracy conditions take the following form:

$$\partial_\eta h = 0, \quad \partial_{uu} h \neq 0, \quad \det \mathrm{d}^2 h > 0, \tag{17}$$

where $\det \mathrm{d}^2 h > 0$ provides information on the curvature of the solution manifold at the singularity. In particular, $\det \mathrm{d}^2 h > 0$ implies that the solution manifold is locally elliptic (see Fig. 3).

Simple bifurcation singularities. They are defined as follows:

$$\partial_\eta h = 0, \quad \partial_{uu} h \neq 0, \quad \det \mathrm{d}^2 h < 0. \tag{18}$$

Here $\det \mathrm{d}^2 h < 0$ implies that the solution manifold is hyperbolic at the singularity, i.e. it locally exhibits a saddle shape (see Fig. 3).

One can recognize that the non-degeneracy condition of the isola and simple bifurcation singularities are tantamount to assessing the curvature of the solution manifold at the singular point [13]. This is similar to the concept of *handedness* of the fold manifold introduced in [45]. Figure 3 illustrate the two scenarii. If the curvature κ is positive, the solution manifold is locally elliptic and level curves with μ fixed defined by Eq. (8) are ellipses, i.e. isolas. If the curvature is negative, the solution manifold is locally hyperbolic and level curves are hyperbolas that intersect each other at the singular point (Fig. 3). Note that with fold bifurcation tracking, the defining conditions are intrinsically enforced. Turning points of the fold curve can be either cusp points, characterized by the coalescence of two fold bifurcations [71] of the bifurcation diagram defined by Eq. 8 and associated to the hysteresis singularity, or simple turning points of the fold curve with respect to the tracking parameter μ. The latter are associated with both isola and simple bifurcation singularities.

The singularities of a vector-valued function can be classified through the study of the defining and non-degeneracy conditions of a scalar function given by Eqs. (15)-(18) by employing the generalized Lyapunov-Schmidt reduction [31,

46, 32]. Govaerts proved in [32] that the derivatives of function h can be computed using bordered matrices in a quite similar fashion to bifurcation tracking. Nevertheless, this method is not straightforward and involves the inversion of several bordered linear systems to compute all the derivatives of interest. Besides, while it could make sense to employ it when carrying out bifurcation with minimally extended systems, it is ill-suited to standard extended systems. Therefore, in the following, we define alternative criteria to characterize codimension-1 singularities.

Hysteresis singularities. At a fold bifurcation of Eq. (8), occurring at a curvilinear abscissa s_0, the Jacobian $\partial_{\mathbf{q}}\boldsymbol{\mathcal{R}}$ has a rank deficiency of one, i.e. there exist vectors $\boldsymbol{\phi}_0$ and $\boldsymbol{\psi}_0$ which span the null spaces of the Jacobian $\partial_{\mathbf{q}}\boldsymbol{\mathcal{R}}$ and its adjoint $\partial_{\mathbf{q}}\boldsymbol{\mathcal{R}}^T$:

$$\partial_{\mathbf{q}}\boldsymbol{\mathcal{R}}\boldsymbol{\phi}_0 = \mathbf{0}, \tag{19}$$

$$\partial_{\mathbf{q}}\boldsymbol{\mathcal{R}}^T\boldsymbol{\psi}_0 = \mathbf{0}. \tag{20}$$

Differentiating Eq. (8) with respect to the curvilinear abscissa and dropping the dependencies in s for clarity reads:

$$\partial_{\mathbf{q}}\boldsymbol{\mathcal{R}}\partial_s\mathbf{q} + \partial_\eta\boldsymbol{\mathcal{R}}\partial_s\eta = \partial_{\mathbf{q}}\boldsymbol{\mathcal{R}}\Delta\mathbf{q} + \partial_\eta\boldsymbol{\mathcal{R}}\Delta\eta = 0 \tag{21}$$

Since $\Delta\eta = 0$ at $s = s_0$, it comes:

$$\Delta\mathbf{q} = \boldsymbol{\phi}_0 \tag{22}$$

Differentiating Eq. (8) twice and using the fact that, at $s = s_0$, $\partial_\eta\boldsymbol{\mathcal{R}}$ is not in the range of $\partial_{\mathbf{q}}\boldsymbol{\mathcal{R}}$ at a fold point, we obtain:

$$\partial_s\Delta\eta = \frac{\boldsymbol{\psi}_0^T\partial_{\mathbf{qq}}\boldsymbol{\mathcal{R}}\boldsymbol{\phi}_0\boldsymbol{\phi}_0}{\boldsymbol{\psi}_0^T\partial_\eta\boldsymbol{\mathcal{R}}} \tag{23}$$

Using the geometric properties of cusp points, we know that $\partial_s\Delta\eta = 0$ at a cusp point. Hence:

$$\boldsymbol{\psi}_0^T\partial_{\mathbf{qq}}\boldsymbol{\mathcal{R}}\boldsymbol{\phi}_0\boldsymbol{\phi}_0 = 0, \tag{24}$$

Since Eq. (24) requires the computation of the Hessian and left and right eigenvectors of the Jacobian, we define a more convenient test function to identify cusp bifurcations from the set of codimension-2 folds:

$$\varphi_{CP} = \begin{cases} \Delta\eta = 0 \\ \Delta\mu = 0 \end{cases} \tag{25}$$

Isola and simple bifurcation singularities. For isola and simple bifurcation singularities, the non-degeneracy condition on the determinant of the Hessian gives information on the local curvature of the solution manifold at a singularity, i.e. at a codimension-2 fold of the tracking curve. Following the concept introduced in [45], the local curvature of the solution manifold can be determined by evaluating the sign of the following scalar, provided the point at which it is evaluated is not a cusp point, i.e. Eq. (25) is non-zero:

$$\varphi_{IS} = -\frac{\boldsymbol{\psi}_0^T\partial_{\mathbf{qq}}\boldsymbol{\mathcal{R}}\boldsymbol{\phi}_0\boldsymbol{\phi}_0}{\boldsymbol{\psi}_0^T\partial_\mu\boldsymbol{\mathcal{R}}\Delta\eta - \boldsymbol{\psi}_0^T\partial_\eta\boldsymbol{\mathcal{R}}\Delta\mu}\left(\partial_s\Delta\eta\Delta\mu - \partial_s\Delta\mu\Delta\eta\right) \tag{26}$$

In this work, the Hessian tensor $\partial_{\mathbf{qq}}\boldsymbol{\mathcal{R}}$ of $\boldsymbol{\mathcal{R}}$, is approximated by finite differences. $\partial_\mu\boldsymbol{\mathcal{R}}$ and $\partial_\eta\boldsymbol{\mathcal{R}}$ arise naturally in the Jacobian of the extended residual computed during bifurcation tracking. $\Delta\eta$ and $\Delta\mu$ are respectively the η and μ-components of the tangent vector of the fold curve, which are easily retrieved from the solver outputs, and $\partial_s\Delta\eta$ and $\partial_s\Delta\mu$ denote the derivative of the η and μ-components of the tangent vector with respect to the arclength which is also easily computed through finite differences. Note that at the exact location of the codimension-2 fold, $\Delta\mu = 0$ and the second term of the denominator of Eq. (26) vanishes. However, it is unlikely to exactly compute such points during the continuation. It follows that the codimension-2 fold is elliptic and thus an isola formation point if Eq. (26) is strictly positive. It is hyperbolic and a point of isola merger if strictly negative.

3. Results and discussion

The objective function may be discontinuous when several IRCs are encountered (see Sect. 3.3). For this reason, a gradient-free algorithm was used. Although the objective function is also, in the general case, expected to be non-convex, in the following, the optimizations were carried out using a local algorithm (the *COBYLA* subroutine from the NLopt.jl Julia package [72]) which appeared to yield satisfactory results. While a comprehensive comparison of various optimization routines falls beyond the scope of this paper, it is worth noting that extending our approach to use global optimization is straightforward.

3.1. Application to a problem with a large number of design variables

We first illustrate the methodology on an optimization problem with a relatively large number of design variables. We consider a finite element model of a cantilever beam of length L with a nonlinear spring with cubic stiffness k_{nl} attached at its free end (Fig. 5). The beam is discretized with Euler-Bernoulli beam elements with one transverse translation and one in-plane rotation per node. The main parameters of the initial model are summarized in Table 1. The nonlinear spring is attached on the translational degree of freedom of the tip node and a harmonic load is applied at 0.21 m from the fixed end.

Table 1
Reference geometrical and mechanical properties of the cantilever beam [74].

Length (m)	Nonlinear coeff. (N/m^3)
0.7	6e9
Width (m)	Height (m)
0.014	0.014
Young's modulus (N/m^2)	Density (kg/m^3)
2.05e11	7800

The vector of optimization variables reads as follows:

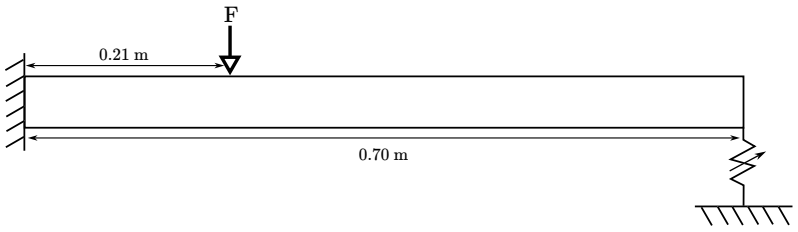

Figure 5: Schematic representation of the cantilever beam [74, 61]

$\boldsymbol{\theta} = (L,\ \mathbf{w}_e^T,\ \mathbf{h}_e^T,\ k_{nl})^T$ where $\mathbf{w}_e$ and $\mathbf{h}_e$ are the vectors of element-wise width and height, i.e. $w_e^{(i)}$ and $h_e^{(i)}$, $i \in [\![1, N_e]\!]$. This amounts to 120 optimization variables. Upper and lower bounds are defined to restrict the optimization to realistic parameter values. The length L is allowed to vary between 0.5 and 0.9 m, the element-wise width and height is bounded between 30% of the reference values and the nonlinear coefficient can vary between 6e8 and 6e10 N/m^3 . To reduce the computational effort, a reduced-order model, which is updated at each iteration of the optimization algorithm, is built using the Craig-Bampton method by retaining both the nonlinear and external forcing degrees of freedom as physical coordinates and five fixed-interface modes. Besides, at each iteration of the optimizer, the damping matrix is updated to maintain modal damping ratios equal to 1% for the first mode and 5% for all subsequent modes. Note that this particular beam model was used as a benchmark for nonlinear system identification in the the European Action COST F3 project and the damping parameters were chosen to ensure consistency with the existing literature [50]. The utilization of a smaller damping term is not expected to introduce any theoretical or conceptual difficulty with the methodology, although it might induce addtional IRCs which could result in an increased computational effort if they were not associated to the same fold bifurcation, as several bifurcation tracking analyses would have to be performed at each iteration of the optimization solver. In this case, one could resort to carrying out bifurcation tracking in parallel to reduce the computational effort. In the following, all computations were carried out with 6 harmonics and 2^8 samples were used to compute the nonlinear forces in the time domain using the alternating frequency/time precedure [9].

A preliminary analysis with the structural parameters of Table 1 reveals the presence of an isola which merges with the main solution branch for sufficiently high amplitudes of the external forcing (see Fig. 6, dashed). The onset (◆) and merger (◆) of the isola are located at $\mu = F = 42$ N and $F = 82$ N, respectively, and lead to a doubling of the amplitude of the resonance peak. Such an isola was demonstrated to be associated to a 3:1 internal resonance between the first and second bending modes of the beam [50, 69].

An optimization was carried out in order to delay the birth of the isola to a target value of 100 N using the objective defined by Eq. (4), with the parameters given in Table 1 as initial guess. 200 iterations were set as the termination criterion. The total computational time amounts to approximately 5 h on a laptop (i7-12700H@2.7 GHz, 16 Gb RAM) running Linux (Fedora 39) and Julia 1.10.1. The average number (rounded to nearest integer) of computed points on the bifurcation tracking curve is equal to 195 and each point on the curve required, on average, 4 iterations of the Newton-like solver to converge.

Figure 6 shows the projection of the fold curves in the frequency-forcing amplitude plane of both the reference and optimized systems with identified singularities. It appears that the point of isola formation (◆) is shifted towards higher forcing amplitudes at the target value of 100 N on the optimized system. Besides, studying singularities provides information on the mechanisms involved in the merger of the isola with the main branch. Fig. 6 shows that the isola merger (◆) occurs at a lower amplitude of the external forcing than the cusp point (◆). This indicates that three codimension-1 folds are created on the main branch as a result of the merger, quickly followed by the coalescence of two of them through a cusp point. Finally, the local curvature of the fold curve of the optimized system appears smaller than that of the initial system. This indicates that, beside delaying the onset of the isola, the optimization decreased the growth rate of the isola with the amplitude of the external forcing. Nonetheless, as the isola formation and merger points are further away from each other compared to the initial system, the isola grows larger before reconnecting with to the main branch, inducing slightly larger frequency and amplitude shifts than for the the initial system.

Figure 7 depicts the geometry of the optimized beam superimposed with the initial geometry in red. The optimized beam has the same length as the reference beam and a nonlinear coefficient equal to 5.99e^9 N/m^3. Furthermore, it has the same width and height except near the clamped end and close to the midspan where both width and height are increased by approximately 15%. The distribution of added material follows the deflection shapes of the first two bending modes, which is coherent with the fact that the isola is associated to a 3:1 modal interaction between those modes. Although, interestingly, the increase in width and height does not affect the same elements. Figure 8a shows the evolution of the value of the objective functional with the number of iterations. One can see that the optimizer requires less than 100 iterations to reach satisfactory values of the objective function. A few outlier points are visible and correspond to changes in length and/or nonlinear coefficient. This suggest a significant sensitivity of the optimization to these two de-

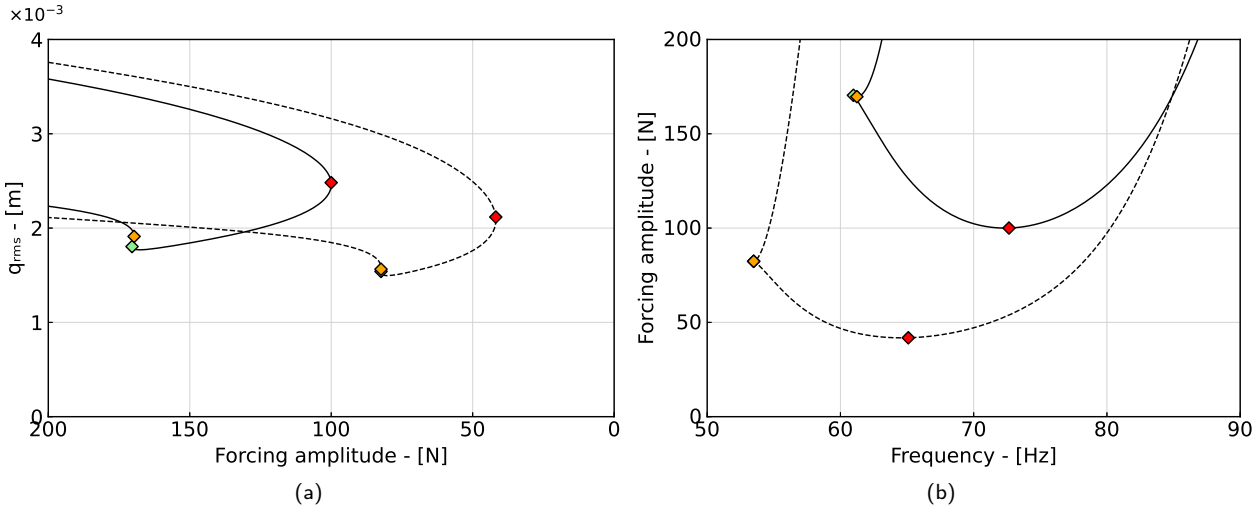

Figure 6: Projections in the amplitude-forcing (a) and forcing-frequency (b) planes of the fold curve of the translation of the beam tip of the reference (- - -) and optimized (——) systems. Cusp bifurcations and points of isola formation and merger are shown in green (◆), red (◆) and orange (◆) diamond markers, respectively.

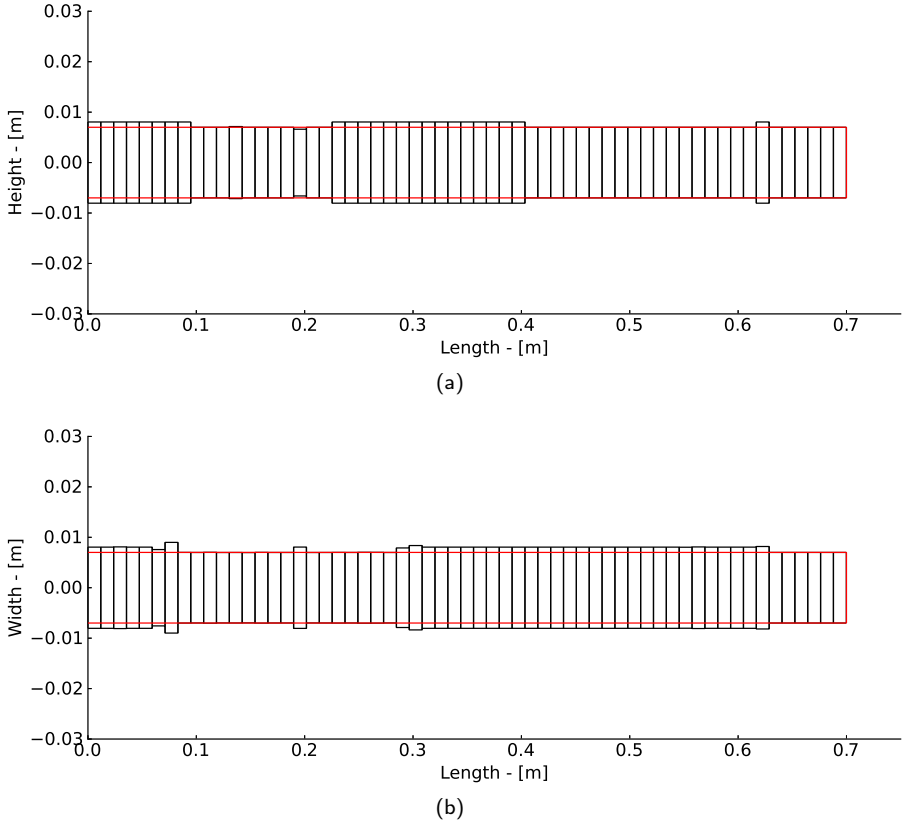

Figure 7: Geometry of the optimized beam. Side view (a) and top view (b). The outline of the reference geometry is displayed in red.

sign variables which could possibly lead to issues related to the robustness of the optimized design. Figure 8b depicts the evolution of the ratio between eigenfrequencies of the second and first bending modes of the underlying linear structure. Although the ratio is larger for the optimized beam, its evolution does not appear to be correlated with the value at which the onset of the isola occurs.

Figure 9 shows the backbone curves of the first and second nonlinear normal modes (NNM) of the initial (Fig 9a) and optimized (Fig 9b) beams. Tongues in the backbone

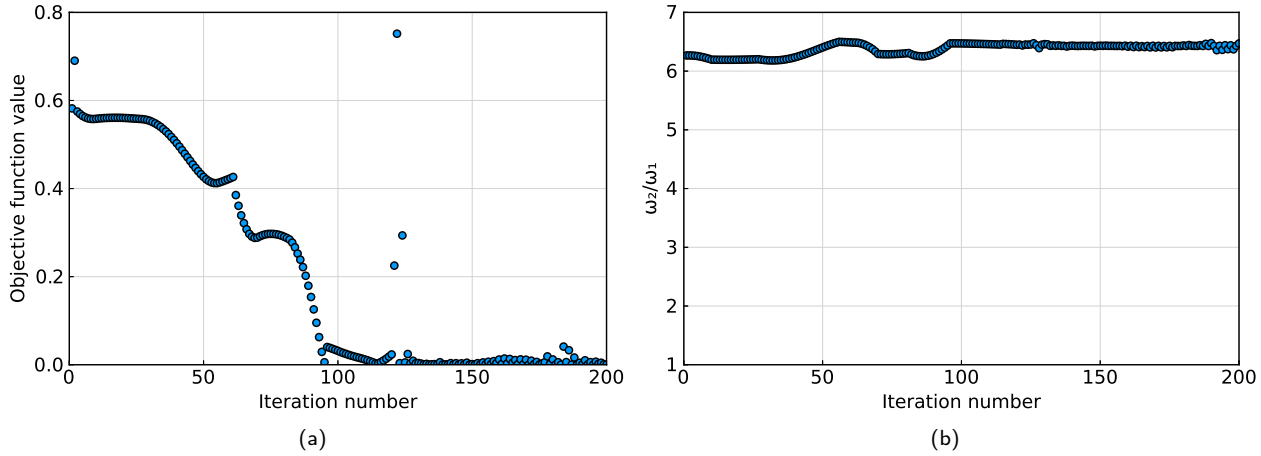

Figure 8: (a) Value of the objective function with respect to the iteration number. (b) Evolution of the ratio of the second and first linear eigenfrequencies with the optimization iterations.

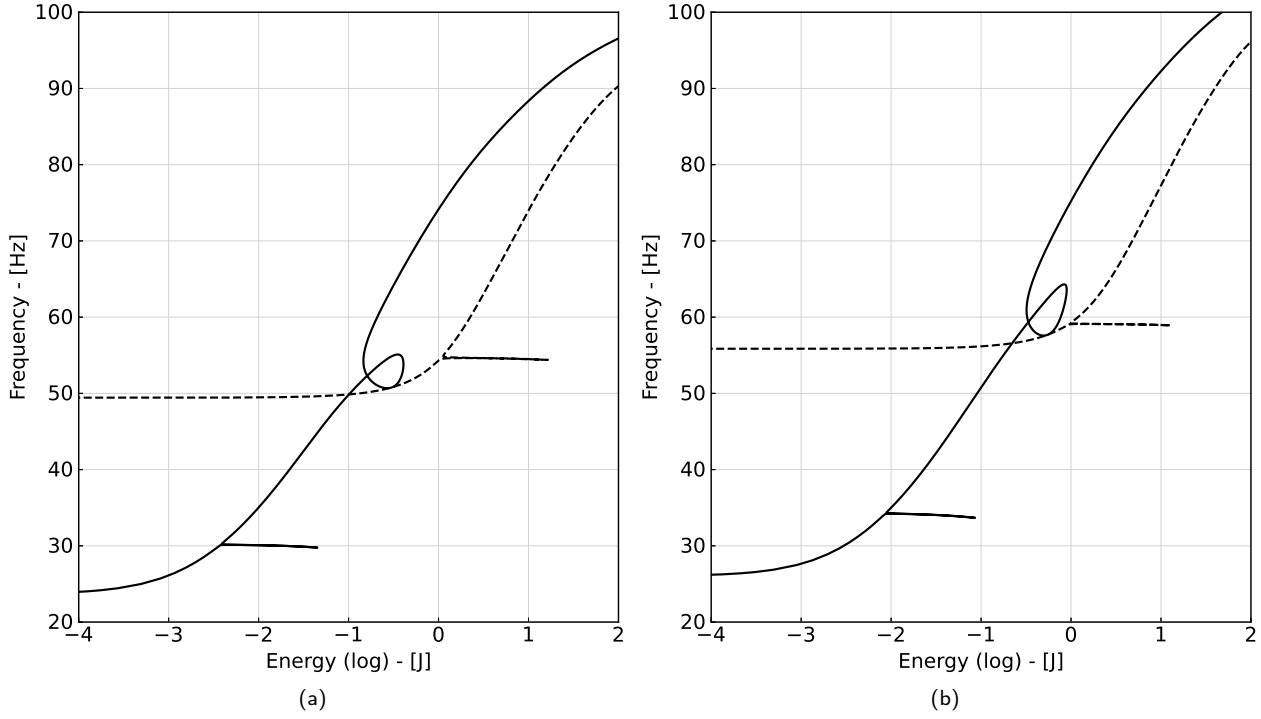

Figure 9: (a) Backbone curves of the first (——) and second (- - -) NNMs of the initial (a) and optimized (b) beams. The frequency of the second NNM has been divided by three to show the 3:1 internal resonance.

curves indicate modal interactions and plotting the backbone of the second mode with its frequency divided by three shows that the modal interaction is a 3:1 internal resonance. One can see from Fig 9a that at low energies, the resonance frequencies of the first and second modes are equal to 23 Hz and 148 Hz, respectively. A similar analysis of Fig 9b reveals that the resonance frequencies of the first and second modes of the optimized beam are shifted towards higher frequencies, with the first one lying at 26 Hz and the second one at 167 Hz. These are quite significant shifts of approximately 13%. Additionally, one can see that the backbone of the first NNM does not exhibit a steeper slope. This indicates that, with the optimized geometry, the 3:1 modal interaction leading to the isola occurs not only at higher energies - approximately $10^{-0.3}$ J compared to $10^{-0.6}$ J for the initial geometry - but also in a more nonlinear regime.

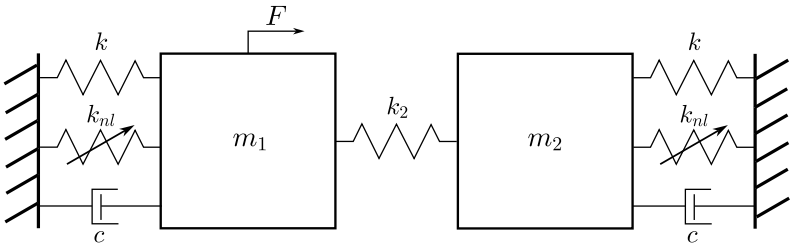

Figure 10: Schematic representation of the mechanical system with considered asymmetries.

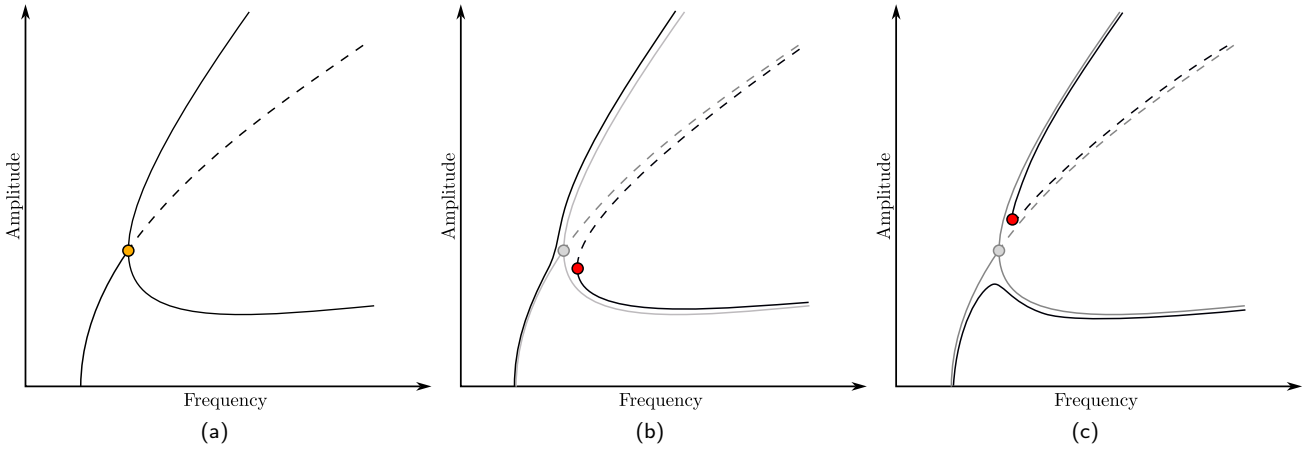

Figure 11: Example of the backbone curve of the second nonlinear mode is the case of perfect symmetry (a) and broken symmetry (b,c). Solid (——) and dashed (- - -) lines indicate stable and unstable responses, respectively. Red (●) and orange (●) circle markers indicate fold bifurcations and branch point (pitchfork), respectively.

3.2. Application to isolas induced by asymmetry

In this section, we consider the control of an isolated response curve induced by a perturbed pitchfork. It is important to note that pitchforks, contrary to the simple bifurcation and isola considered before, are singularities of codimension-2 so that their study requires the variation of two unfolding parameters. However, in the degenerate case of a system exhibiting Z_2-symmetry, pitchforks are singularities of codimension-0, meaning they are as generic as fold bifurcations on a FRC. This has important consequences since numerical models are often an idealization with symmetry, either due to perfect geometries or simplifying assumptions. Consequently, when even a slight asymmetry is introduced, the pitchfork which connects different solution branches is annihilated and the resulting bifurcation diagram exhibits an isolated response curve.

We consider a 2-degree of freedom system (see Fig. 10) modelled by the following equation:

$$\begin{bmatrix} m_1 & 0 \\ 0 & m_2 \end{bmatrix} \begin{pmatrix} \ddot{q}_1 \\ \ddot{q}_2 \end{pmatrix} + \begin{bmatrix} c & 0 \\ 0 & c \end{bmatrix} \begin{pmatrix} \dot{q}_1 \\ \dot{q}_2 \end{pmatrix} + \begin{bmatrix} k+k_2 & -k_2 \\ -k_2 & k+k_2 \end{bmatrix} \begin{pmatrix} q_1 \\ q_2 \end{pmatrix} + \begin{pmatrix} k_{nl} \\ k_{nl} \end{pmatrix} \begin{pmatrix} q_1^3 \\ q_2^3 \end{pmatrix} = \begin{pmatrix} F\cos(\Omega t) \\ 0 \end{pmatrix} \tag{27}$$

The symmetric system exhibits two NNMs corresponding to the in-phase and out-of-phase displacements of the two masses. The backbone curve of the second NNM bifurcates at a pitchfork, resulting in two mixed NNMs whose shapes exhibit contributions from both the in-phase and out-of-phase NNMs. We refer the interested reader to [41] for more details. As illustrated in Fig. 11, when symmetry is broken, e.g. by applying an asymmetric forcing or setting $m_1 \neq m_2$, the pitchfork degenerates into a primary backbone and isolated backbone. The branch which becomes isolated depends on the asymmetry introduced in the system [43]. In the following we consider two cases illustrating both scenarii.

3.2.1. Asymmetric forcing

In this first example, the symmetry of the system is broken by applying an external periodic load F only on the first degree of freedom and the masses of the two degrees of freedom are equal $m_1 = m_2$. This leads to the lower branch of the bifurcated second NNM induced by the pitchfork to become isolated (see Fig. 11b). Figure 12 shows two FRCs computed at $F = 1.5$ N (Fig. 12a) and $F = 2$ N (Fig. 12b), illustrating the merging scenario. The FRC first develops around the backbone of the second NNM (Fig. 12a) located around 3.5 rad/s. Once the forcing amplitude reaches a sufficiently

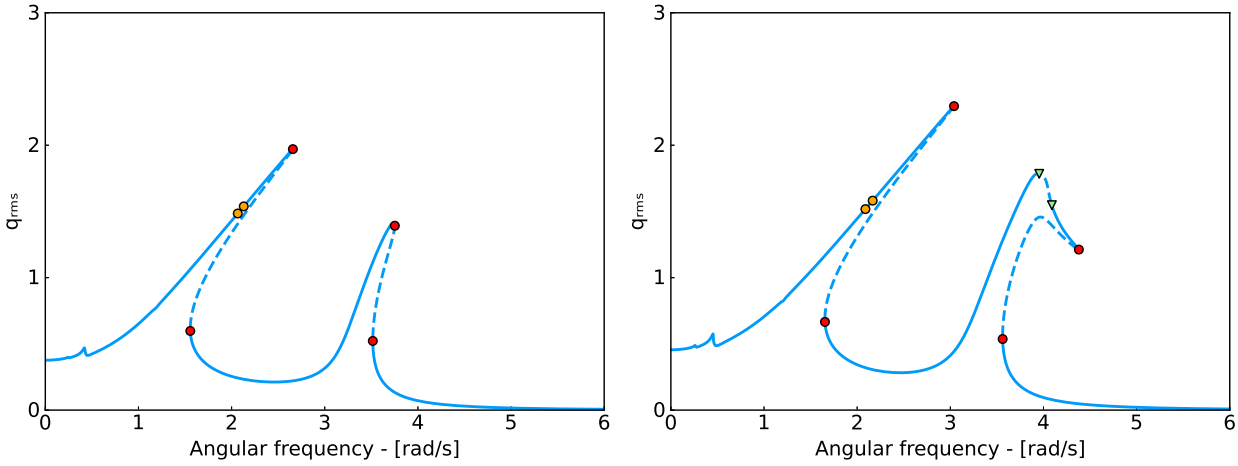

(a) $F = 1.5$ N (b) $F = 2$ N

Figure 12: Forced response curves of the second degree of freedom with asymmetric forcing before (a) and after isola merger (b). Stable and unstable responses are traced in solid (——) and dashed (- - -) lines, respectively. Folds and branch points are denoted by red (●) and orange (●) circle markers, respectively, and Neimark-Sacker bifurcations are shown in green (▼) triangle markers.

high value, the isola supported by the lower branch of the perturbed pitchfork merges with the main solution branch without creating additional fold bifurcations and the FRC exhibits a downward-pointing peak.

Figure 13 shows the FRC around the second mode and fold tracking curve of the initial system with asymmetric forcing. One can see that the FRC exhibits a complicated behaviour with three resonance peaks, six fold and two Neimark-Sacker bifurcations. Carrying out bifurcation tracking starting from the fold with smallest amplitude reveals one cusp bifurcation and points of isola formation and merger. One can see that the former occurs at a lower value of the forcing amplitude ($F = 0.57$ N) than the latter ($F = 1.839$ N and $F = 1.847$ N, respectively) which shows that a bi-stable zone induced by fold bifurcations is created before the onset and merger of the isola. Note that this is coherent with Fig. 12a which shows the two folds on the FRC supported by the backbone of the second NNM. Moreover, one can see that the points of isola formation and merger are almost coincident and the curvature at the point of isola formation is relatively high, indicating that the multi-stable zone induced by the IRC is relatively small. The implications are twofold: the amplitude and frequency shifts induced by the isola when it merges with the main branch are minor and the isola would, in practice, be quite difficult to observe in physical experiments.

An optimization is carried out for this isola. The initial guess for the optimization procedure is chosen as the parameters used to compute Fig. 12-13, i.e. $m_1 = m_2 = 1$, $k = 1$, $k_2 = 5$, $c = 0.1$ and $k_{nl} = 1$. The vector of optimization variables is defined as $x = (k, k_2, k_{nl})^T$ with each variable allowed to vary between 50% of its initial value. No termination criterion is defined apart from the number of optimization iterations set to 200.

Figure 14 shows the projection in the forcing-frequency (Fig. 14a) and amplitude-forcing (Fig. 14b) planes of the fold curves of the second degree of freedom of the system with initial and optimized parameters $k = 1.5$, $k_2 = 7.5$ and $k_{nl} = 0.5$. One can see that the system with optimized parameters still exhibits an IRC which merges with the main branch for sufficiently high forcing amplitudes. Similarly to the initial system, the points of isola formation and merger are close to one another. The frequencies at which the isola is created and merges with the main branch are shifted to higher values (approximately $\Omega = 5$ rad/s for both). Furthermore, both the onset and merger of the isola are delayed to forcing amplitudes close to $F = 4$ N, i.e. a 100% increase compared to the initial system. Note that, although the cusp bifurcation giving birth to the two folds on the FRC supported by the second NNM is delayed ($F = 1.08$ N compared to $F = 0.57$ N), the fact that the points of isola formation and merger exhibit a larger shift may suggest that, for a given forcing amplitude, the response amplitude is actually higher for the optimized system.

On this example, the total computational time for 200 iterations amounts to approximately 40 min. The average number (rounded to nearest integer) of computed points on the bifurcation tracking curve is equal to 175 and each point on the curve required, on average, 3 iterations of the Newton-like solver to converge.

3.2.2. Asymmetric forcing and mass

We now consider both asymmetric forcing on the first degree of freedom and an asymmetric mass with $m_1 = 1$ and $m_2 = 1.1$. Figure 15 shows that in this case, the isolated backbone corresponds to the upper branch of the pitchfork (see Fig. 11c).

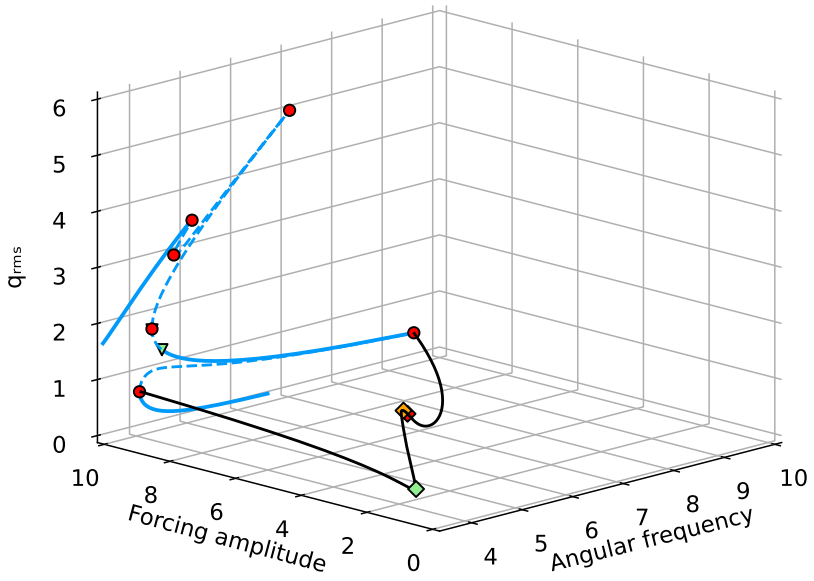

Figure 13: Forced response and fold bifurcation curves of the second degree of freedom with asymmetric forcing on the first degree of freedom. Stable and unstable responses are traced in solid (——) and dashed (- - -) lines, respectively. Folds and branch points are denoted by red (●) and orange (●) circle markers, respectively, and Neimark-Sacker bifurcations are shown in green (▼) triangle markers. Green (◆), red (◆) and orange (◆) diamond markers represent cusp bifurcations and points of isola formation and merger, respectively.

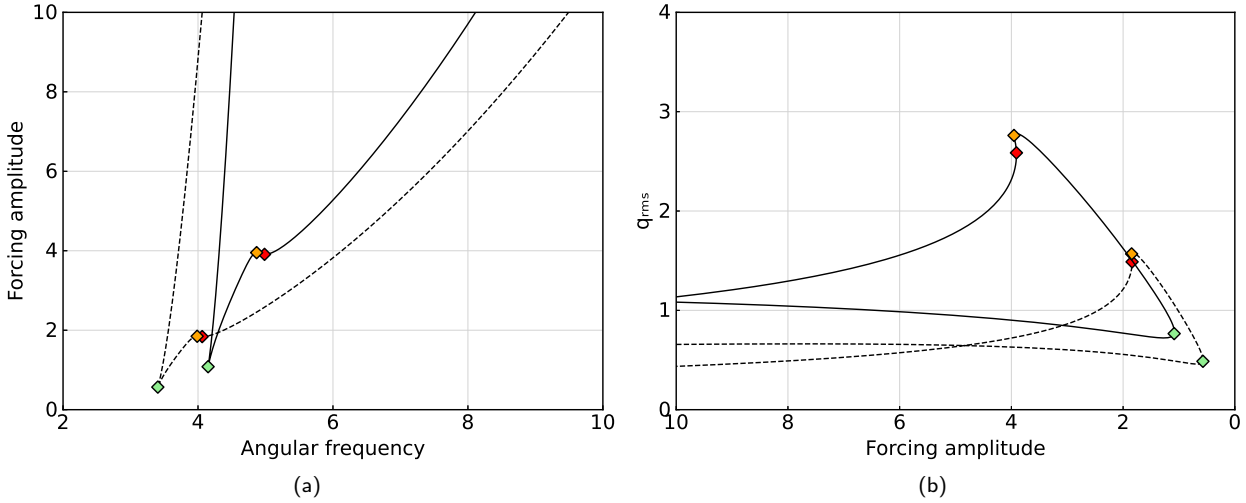

Figure 14: Projections in the forcing-frequency (a) and amplitude-forcing (b) planes of the fold curve of the second degree of freedom of the reference (- - -) and optimized (——) systems with asymmetric forcing. Cusp bifurcations and points of isola formation and merger are shown in green (◆), orange (◆) and red (◆) diamond markers, respectively.

In particular, Figures 15a-15b show two FRCs computed just before the merger point at $F = 3.5$ N and almost exactly on the merger point at $F = 4.038$ N, respectively. One can see on Fig. 15a that the FRC first develops around the backbone connected to the lower branch of the perturbed pitchfork and that, for sufficiently high forcing amplitudes, an IRC connects to the peak of the resonance located at approximately $\Omega = 3.5$ rad/s through a branch point corresponding to a transcritical bifurcation (see Fig. 15b). Contrary to the previous example, the merging isola has important consequences as it induces a large increase in the response amplitude at resonance which may have dire consequences for the

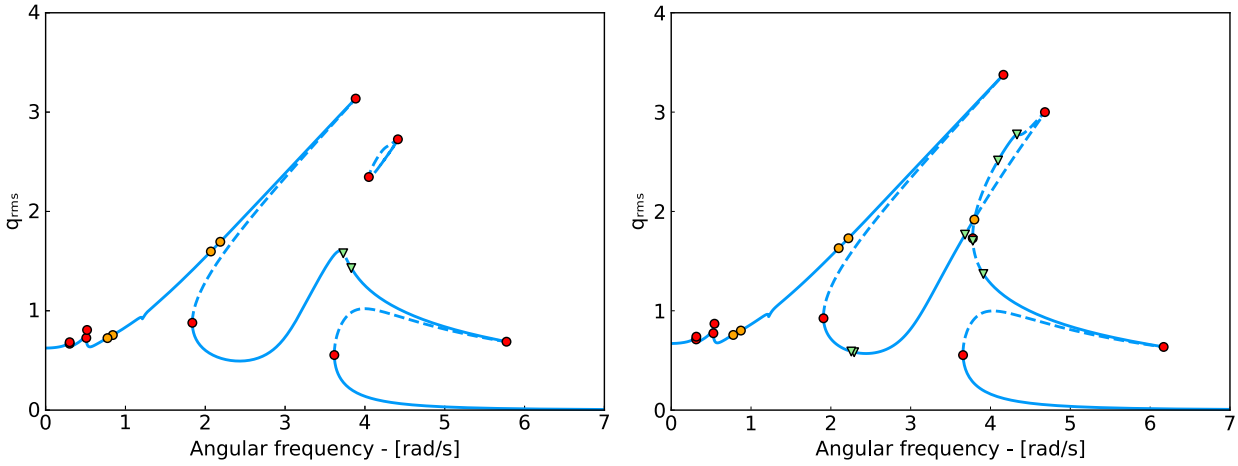

(a) $F = 3.5$ N (b) $F = 4.038$ N

Figure 15: Forced response curve of the second degree of freedom with asymmetric forcing and mass before isola merger (a) and after merger (b). Stable and unstable responses are traced in solid (——) and dashed (- - -) lines, respectively. Folds and branch points are denoted by red (●) and orange (●) circle markers, respectively, and Neimark-Sacker bifurcations are shown in green (▼) triangle markers.

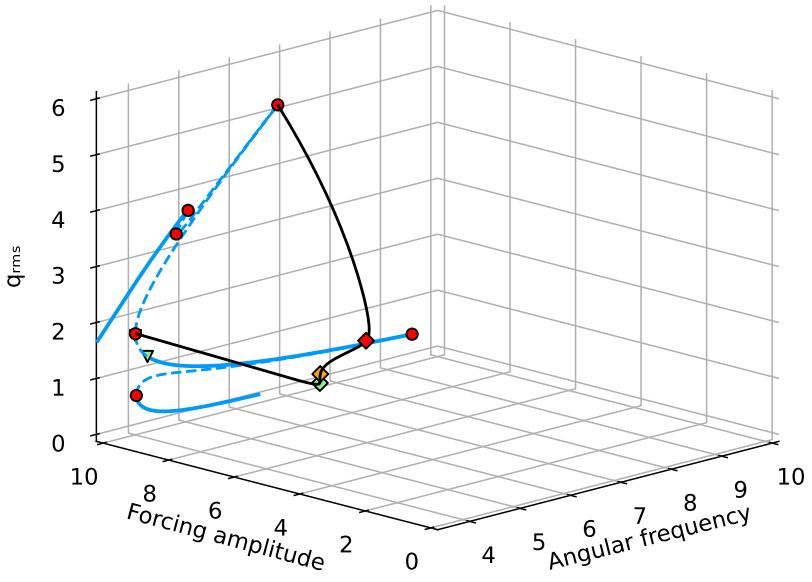

Figure 16: Forced response and fold bifurcation curves of the second degree of freedom with asymmetric forcing and mass. Stable and unstable responses are traced in solid (——) and dashed (- - -) lines, respectively. Folds and branch points are denoted by red (●) and orange (●) circle markers, respectively, and Neimark-Sacker bifurcations are shown in green (▼) triangle markers. Green (◆), red (◆) and orange (◆) diamond markers represent cusp bifurcations and points of isola formation and merger, respectively.

structural integrity of the system.

Figure 16 shows the FRC around the second mode and fold tracking curve of the initial system with asymmetric forcing and mass. One can see that the FRC is almost identical to the one computed with only an asymmetric forcing (see Fig. 13). This indicates that the computation was carried out sufficiently far away from the value of forcing amplitude of the isola merger that the system behaves as if the pitchfork were not perturbed. Moreover, following the evolution of the highest amplitude fold bifurcation reveals that the merging scenario is different from the previous case. Indeed, the isola is this time supported by the upper branch of

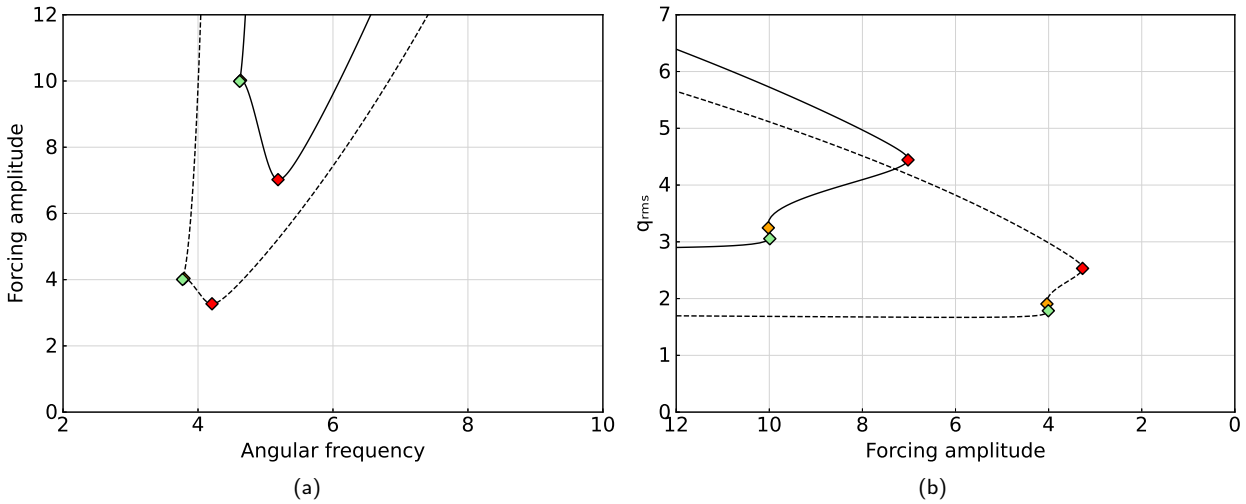

Figure 17: Projections in the forcing-frequency (a) and amplitude-forcing (b) planes of the fold curve of the second degree of freedom of the reference (- - -) and optimized (——) systems with asymmetric forcing and mass. Cusp bifurcations and points of isola formation and merger are shown in green (◆), red (◆) and orange (◆) diamond markers, respectively.

the pitchfork. One can see that, in terms of forcing amplitudes, the cusp bifurcation lies between the points of isola formation and merger, indicating that the isola merger occurs through the coalescence of two fold bifurcations.

Figure 17 shows the projection in the forcing-frequency (Fig. 17a) and amplitude-forcing (Fig. 17b) planes of the fold curves (shown in Fig. 16) of the second degree of freedom of the system with initial and optimized parameters $k = 1.5$ $k_2 = 7.5$ and $k_{nl} = 0.5$ which, interestingly, exactly match those of the optimized system with only the forcing as asymmetry. Besides, both isola formation and merger occur at higher values of forcing amplitudes compared to the previous case with only asymmetric forcing. Furthermore, the optimization allows one to significantly delay the birth of the isola as well as the isola merger and cusp bifurcation. However the optimization leads to an increased distance between the points of isola formation and merger, resulting in a larger interval of forcing amplitudes affected by the isola-induced multi-stability.

3.3. Application to multiple IRCs with modal interactions

In this section, we apply the proposed methodology to a system exhibiting multiple IRCs to demonstrate its broad applicability. We consider a 2-degree-of-freedom base-excited mechanical system, studied in [18], whose schematic representation is visible in Fig. 18. The equations of motion of the system are:

$$\begin{bmatrix} m_1 & 0 \\ 0 & m_2 \end{bmatrix} \begin{pmatrix} \ddot{q_1} \\ \ddot{q_2} \end{pmatrix} + \begin{bmatrix} c_1 & 0 \\ 0 & c_2 \end{bmatrix} \begin{pmatrix} \dot{q_1} \\ \dot{q_2} \end{pmatrix} + \begin{bmatrix} k_1 + k_2 & -k_2 \\ -k_2 & k_2 + k_3 \end{bmatrix} \begin{pmatrix} q_1 \\ q_2 \end{pmatrix} + \begin{pmatrix} f_{nl}(q_1) \\ 0 \end{pmatrix} = \begin{pmatrix} 0 \\ 0 \end{pmatrix} \tag{28}$$

where q, m, c, and k are displacement, mass, damping and stiffness terms, respectively. Subscripts 1 and 2 denote the degree of freedom number. The nonlinear force is noted f_{nl}. This force stems from two transverse springs with stiffness k (Fig. 18) attached to the first mass. External excitation is applied through the prescribed sinusoidal motion of the base of the transverse springs. By performing a Taylor series expansion, it can be shown that for small amplitudes the nonlinear force assumes the following polynomial form [18]:

$$f_{nl}(q_1) = 2k(1-\lambda)\left(q_1 - d\sin(\Omega t)\right) + \frac{k\lambda}{l^2}\left(q_1 - d\sin(\Omega t)\right)^3 \tag{29}$$

where d is the amplitude of the base excitation, l the length of the transverse springs and λ a prestress parameter.

Table 2
Reference mechanical properties of the base-excited system

m_1	m_2	k_1	k_2	k_3
3.49	0.46	135.0	261.8	485.6
k	l	λ	c_1	c_2
503.7	$3.5e^{-2}$	0.98	2.25	$8.5e^{-2}$

Figures 19a-19b show the fold curve of the system with parameters reported in Table 2. It appears that two points of isola formation (◆), two points of isola merger (◆) and one cusp bifurcation (◆) are visible. The latter corresponds to the onset of bi-stability on the primary resonance induced by two fold bifurcations. The presence of two points of isola formation indicates that two isolas are created at different values of the amplitude of the base excitation. One can see that the first isola creation, located at $d = 2.3e^{-3}$ m, occurs at a higher amplitude than the second one. Besides, the curvature of the fold curve is much smaller than around the

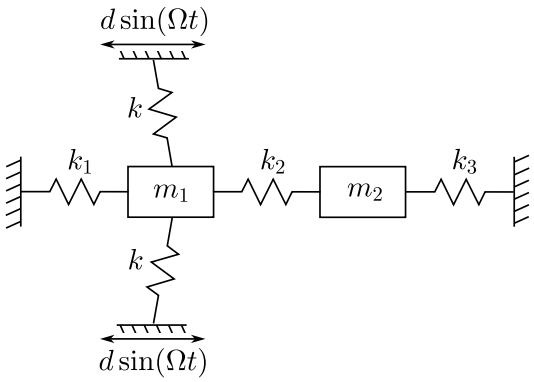

Figure 18: Schematic representation of the considered mechanical system [18].

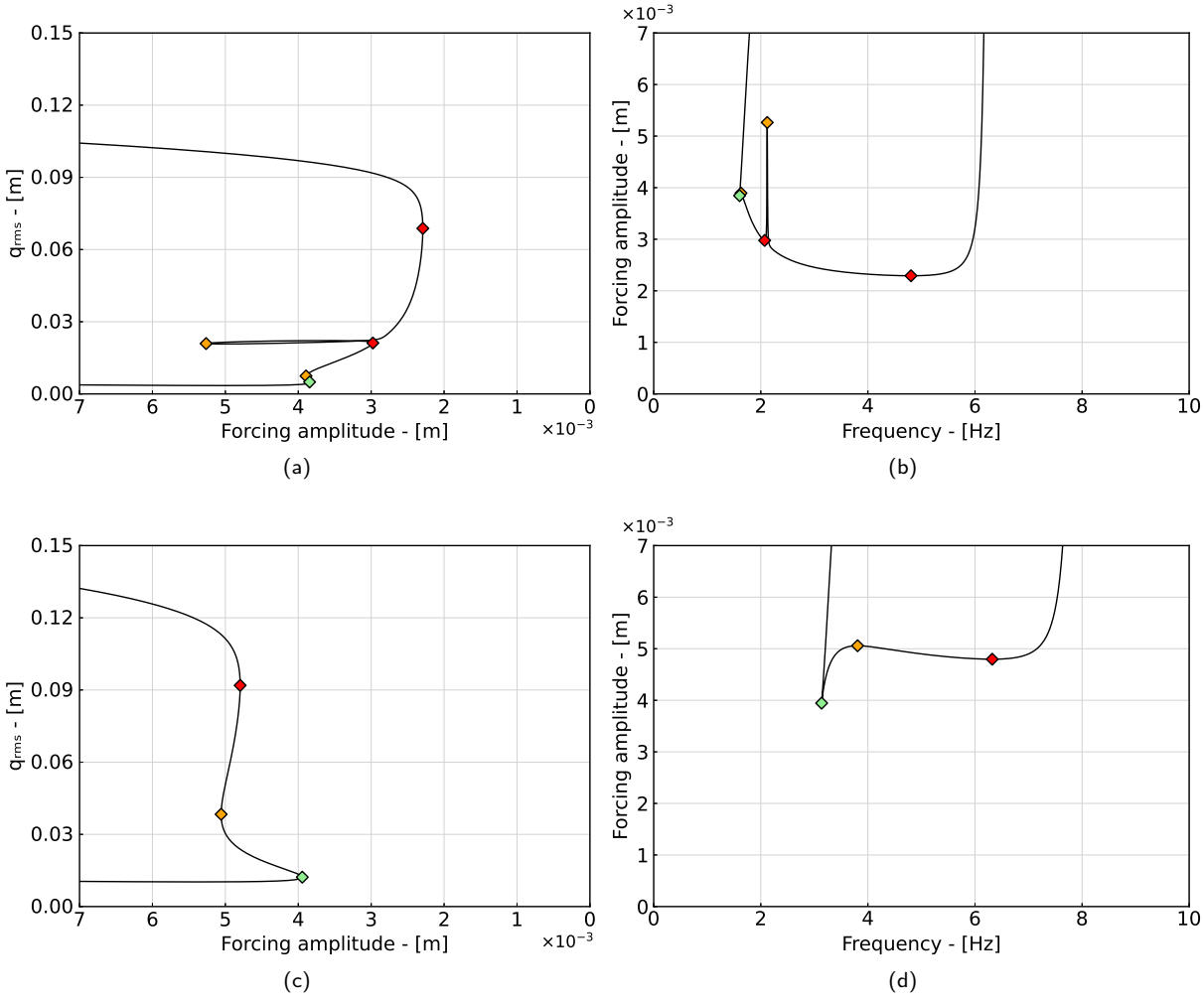

Figure 19: Fold curve of the reference (a,b) and optimized (c,d) systems. Cusp bifurcations and points of isola formation and merger are denoted by green (◆), red (◆) and orange (◆) diamond markers, respectively.

second point of isola formation, indicating an extremely fast growth. This leads to a bi-stable zone where low-amplitude responses co-exist with extremely high-amplitude ones. Regarding the points of isola merger, the first one occurs shortly after the cusp bifurcation, and leads to the increase of the resonance amplitude from approximately $7e^{-3}$ m to approximately $2.2e^{-2}$ m. The second point of isola merger occurs at $d = 5.3e^{-3}$ m and leads to a dramatic increase of the resonance amplitude to almost $1.0e^{-1}$ m. This merger, as well as the formation of the low-amplitude isola, appear to be

induced by a 3:1 modal interaction with the second mode, as suggested by the almost straight line formed by the fold curve at approximately $\Omega = 2.1$ Hz. Indeed, this straight line indicates that both the amplitude of the main branch and isola saturate. This phenomenon has been often reported to be characteristic of modal coupling [5, 18].

An optimization can be carried out in order to maximize the minimum amplitude of base displacement at which the first isola is created to prevent isola-induced multistability (Eq. (2)). Since multiple isolas can occur, we resort to using a bound formulation [60] for the optimization problem. Suppose that N points of isola formation are detected on the fold curve, the objective functional is expressed as:

$$\underset{\boldsymbol{\theta}}{\text{maximize}} \quad \mathcal{F} = \min(\mu_{birth}^{(k)}) \quad \forall k \in [1, N] \tag{30}$$

The design variables considered for the optimization are the two masses m_1 and m_2, the three springs k_1, k_2 and k_3 as well as the transverse springs parameters k, l and λ. Variables m_1, m_2, k_1, k_2 and k_3 are allowed to vary within 50% of their reference values. The parameters of the transverse springs are bounded between 20% of their reference values except λ which can vary between 0.784 and 0.98 N/m.

Fig. 19c-19d show the fold curve computed with the optimized system parameters ($m_1 = 1.745$ kg, $m_2 = 0.431$ kg, $k_1 = 202.5$ N/m, $k_2 = 392.7$ N/m and $k_3 = 687.781$ N/m, $k = 402.96$ N/m, $l = 0.042$ m and $\lambda = 0.784$). One can see that only the high-amplitude isola induced by modal interaction persists. The point of isola formation is shifted towards higher values of the amplitude of the base excitation ($d = 4.8\text{e}^{-3}$). Besides, the point of isola merger appears relatively unaffected by the optimization as it occurs at $d = 5.1\text{e}^{-3}$ m although the associated amplitude is higher. Overall, all singular points lie at a higher amplitude compared to the fold curve of the initial system. For instance, the amplitude of the point of isola formation of the optimized system is 0.085 m compared to 0.07 for the initial system.

4. Concluding remarks

Isolated response curves are important nonlinear phenomena that can have important consequences on the performances and structural integrity of a mechanical system. In this paper, we introduced a general methodology to control the location of such curves in a codimension-2 bifurcation diagram. Using three examples of varying complexity, we demonstrated that our methodology can handle large-scale optimization problems with more than a hundred variables as well as complicated mechanical systems exhibiting multiple isolas.

Although we chose the harmonic balance method to compute periodic solutions for its performances, the methodology is quite general and can be adapted to other discretization techniques such as the shooting or orthogonal collocation methods with minimal effort. Besides, special attention was taken to ensure that our methodology was not only limited to bifurcation tracking analyses carried out with minimally extended systems but also to standard extended systems.

The main challenge of our methodology lies in providing the bifurcation tracking solver with an initial guess located on an isola. Future work could explore the use of deflated continuation techniques in order to improve the robustness of the methodology.

References

[1] Abramson, H.N., 1955. Response curves for a system with softening restoring force. Journal of Applied Mechanics 22, 434–435. doi:10.1115/1.4011105.

[2] Alcorta, R., Baguet, S., Prabel, B., Piteau, P., Jacquet-Richardet, G., 2019. Period doubling bifurcation analysis and isolated subharmonic resonances in an oscillator with asymmetric clearances. Nonlinear Dynamics 98, 2939–2960. doi:https://doi.org/10.1007/s11071-019-05245-6.

[3] Alexander, N.A., Schilder, F., 2009. Exploring the performance of a nonlinear tuned mass damper. Journal of Sound and Vibration 319, 445–462. URL: https://www.sciencedirect.com/science/article/pii/S0022460X08004823, doi:https://doi.org/10.1016/j.jsv.2008.05.018.

[4] Allgower, E.L., Schwetlick, H., 1997. A general view of minimally extended systems for simple bifurcation points. ZAMM - Journal of Applied Mathematics and Mechanics / Zeitschrift für Angewandte Mathematik und Mechanik 77, 83–97. doi:https://doi.org/10.1002/zamm.19970770203.

[5] Antonio, D., Zanette, D.H., López, D., 2012. Frequency stabilization in nonlinear micromechanical oscillators. Nature Communications 3, 806. URL: https://doi.org/10.1038/ncomms1813, doi:10.1038/ncomms1813.

[6] Bayer, F., Leine, R.I., 2023. Sorting-free Hill-based stability analysis of periodic solutions through Koopman analysis. Nonlinear Dynamics 111, 8439–8466. URL: https://doi.org/10.1007/s11071-023-08247-7, doi:10.1007/s11071-023-08247-7.

[7] Boullé, N., Farrell, P.E., Rognes, M.E., 2023. Optimization of hopf bifurcation points. SIAM Journal on Scientific Computing 45, B390–B411. URL: https://doi.org/10.1137/22M1474448, doi:10.1137/22M1474448.

[8] Boullé, N., Farrell, P.E., Paganini, A., 2022. Control of Bifurcation Structures using Shape Optimization. SIAM Journal on Scientific Computing 44, A57–A76. URL: https://doi.org/10.1137/21M1418708, doi:10.1137/21M1418708.

[9] Cameron, T.M., Griffin, J., 1989. An Alternating Frequency/Time Domain Method for Calculating the Steady-State Response of Nonlinear Dynamic Systems. Journal of Applied Mechanics. doi:https://doi.org/10.1115/1.3176036.

[10] Capecchi, D., Vestroni, F., 1990. Periodic response of a class of hysteretic oscillators. International Journal of Non-Linear Mechanics 25, 309–317. URL: https://www.sciencedirect.com/science/article/pii/002074629090060M, doi:https://doi.org/10.1016/0020-7462(90)90060-M.

[11] Cirillo, G., Habib, G., Kerschen, G., Sepulchre, R., 2017. Analysis and design of nonlinear resonances via singularity theory. Journal of Sound and Vibration 392, 295–306. URL: https://www.sciencedirect.com/science/article/pii/S0022460X16308057, doi:https://doi.org/10.1016/j.jsv.2016.12.044.

[12] D'Anna, A., Lignola, P.G., Scott, S.K., Gray, P., 1986. The application of singularity theory to isothermal autocatalytic open systems: the elementary scheme a + mb = (m + 1)b. Proceedings of the Royal Society A. Mathematical and Physical Sciences 403, 341–363. doi:10.1098/rspa.1986.0015.

[13] Dellwo, D., Keller, H.B., Matkowsky, B.J., Reiss, E.L., 1982. On the birth of isolas. SIAM Journal on Applied Mathematics 42, 956–963. doi:10.1137/0142068.

[14] Dellwo, D.R., 1986. A constructive theory of isolas supported by

parabolic cusps, centers and bifurcation points. SIAM Journal on Applied Mathematics 46, 740–764. doi:10.1137/0146048.

[15] Denimal, E., El Haddad, F., Wong, C., Salles, L., 2021. Topological Optimization of Under-Platform Dampers With Moving Morphable Components and Global Optimization Algorithm for Nonlinear Frequency Response. Journal of Engineering for Gas Turbines and Power 143. doi:10.1115/1.4049666. 021021.

[16] Denimal, E., Renson, L., Wong, C., Salles, L., 2022. Topology optimisation of friction under-platform dampers using moving morphable components and the efficient global optimization algorithm. Structural and Multidisciplinary Optimization 65, 56. URL: https://doi.org/10.1007/s00158-021-03158-w, doi:10.1007/s00158-021-03158-w.

[17] Detroux, T., Noël, J.P., Kerschen, G., 2021. Tailoring the resonances of nonlinear mechanical systems. Nonlinear Dynamics 103, 3611–3624. URL: https://doi.org/10.1007/s11071-020-06002-w, doi:10.1007/s11071-020-06002-w.

[18] Detroux, T., Noël, J.P., Virgin, L.N., Kerschen, G., 2018. Experimental study of isolas in nonlinear systems featuring modal interactions. PLOS ONE 13, 1–25. URL: https://doi.org/10.1371/journal.pone.0194452, doi:10.1371/journal.pone.0194452.

[19] Detroux, T., Renson, L., Masset, L., Kerschen, G., 2015. The harmonic balance method for bifurcation analysis of large-scale nonlinear mechanical systems. Computer Methods in Applied Mechanics and Engineering 296, 18–38. doi:https://doi.org/10.1016/j.cma.2015.07.017.

[20] Doedel, E.J., Oldeman, B.E., Pando L., C.L., 2011. Bifurcation structures in a model of a CO_2 laser with a fast saturable absorber. International Journal of Bifurcation and Chaos 21, 305–322. doi:10.1142/S021812741102843X.

[21] Dou, S., Jensen, J.S., 2015. Optimization of nonlinear structural resonance using the incremental harmonic balance method. Journal of Sound and Vibration 334, 239–254. URL: https://www.sciencedirect.com/science/article/pii/S0022460X14006956, doi:https://doi.org/10.1016/j.jsv.2014.08.023.

[22] Dou, S., Strachan, B.S., Shaw, S.W., Jensen, J.S., 2015. Structural optimization for nonlinear dynamic response. Philosophical Transactions of the Royal Society A: Mathematical, Physical and Engineering Sciences 373, 20140408. URL: https://royalsocietypublishing.org/doi/abs/10.1098/rsta.2014.0408, doi:10.1098/rsta.2014.0408.

[23] Duan, C., Rook, T.E., Singh, R., 2007. Sub-harmonic resonance in a nearly pre-loaded mechanical oscillator. Nonlinear Dynamics 50, 639–650. URL: https://doi.org/10.1007/s11071-006-9185-y, doi:10.1007/s11071-006-9185-y.

[24] Erneux, T., Reiss, E.L., 1983. Brussellator isolas. SIAM Journal on Applied Mathematics 43, 1240–1246. doi:10.1137/0143082.

[25] Farrell, P.E., Beentjes, C.H.L., Birkisson, A., 2016. The computation of disconnected bifurcation diagrams. arXiv:1603.00809.

[26] Farrell, P.E., Birkisson, A., Funke, S.W., 2015. Deflation Techniques for Finding Distinct Solutions of Nonlinear Partial Differential Equations. SIAM Journal on Scientific Computing 37, A2026–A2045. URL: https://doi.org/10.1137/140984798, doi:10.1137/140984798.

[27] Fink, J.P., Rheinboldt, W.C., 1986. Folds on the solution manifold of a parametrized equation. SIAM Journal on Numerical Analysis 23, 693–706. doi:10.1137/0723045.

[28] Fontanela, F., Vizzaccaro, A., Auvray, J., Niedergesäß, B., Grolet, A., Salles, L., Hoffmann, N., 2021. Nonlinear vibration localisation in a symmetric system of two coupled beams. Nonlinear Dynamics 103, 3417–3428. URL: https://doi.org/10.1007/s11071-020-05760-x, doi:10.1007/s11071-020-05760-x.

[29] Förster, A., Krack, M., 2016. An efficient method for approximating resonance curves of weakly-damped nonlinear mechanical systems. Computers & Structures 169, 81–90. URL: https://www.sciencedirect.com/science/article/pii/S0045794916300499, doi:https://doi.org/10.1016/j.compstruc.2016.03.003.

[30] Gobat, G., Guillot, L., Frangi, A., Cochelin, B., Touzé, C., 2021. Backbone curves, Neimark-Sacker boundaries and appearance of quasi-periodicity in nonlinear oscillators: application to 1:2 internal resonance and frequency combs in MEMS. Meccanica 56, 1937–1969. URL: https://doi.org/10.1007/s11012-021-01351-1, doi:10.1007/s11012-021-01351-1.

[31] Golubitsky, M., Schaeffer, D.G., 1984. Singularities and Groups in Bifurcation Theory. Springer New York, NY. doi:https://doi.org/10.1007/978-1-4612-5034-0.

[32] Govaerts, W., 1995. Bordered matrices and singularities of large nonlinear systems. International Journal of Bifurcation and Chaos 05, 243–250. doi:10.1142/S0218127495000181.

[33] Govaerts, W., 2000. Numerical bifurcation analysis for odes. Journal of Computational and Applied Mathematics 125, 57 – 68. doi:https://doi.org/10.1016/S0377-0427(00)00458-1.

[34] Govaerts, W., Kuznetsov, Y., Dhooge, A., 2005. Numerical continuation of bifurcations of limit cycles in matlab. SIAM Journal ON Scientific Computing 27, 231–252.

[35] Govaerts, W., Sijnave, B., 1999. Matrix manifolds and the jordan structure of the bialternate matrix product. Linear Algebra and its Applications 292, 245 – 266. doi:https://doi.org/10.1016/S0024-3795(99)00039-7.

[36] Grenat, C., Baguet, S., Lamarque, C.H., Dufour, R., 2019. A multiparametric recursive continuation method for nonlinear dynamical systems. Mechanical Systems and Signal Processing 127, 276–289. doi:https://doi.org/10.1016/j.ymssp.2019.03.011.

[37] Grenat, C., Baguet, S., Lamarque, C.H., Dufour, R., 2022. Mass sensing by symmetry breaking and localization of motion in an array of electrostatically coupled nonlinear MEMS resonators. International Journal of Non-Linear Mechanics 140, 103903. URL: https://www.sciencedirect.com/science/article/pii/S0020746221002171, doi:https://doi.org/10.1016/j.ijnonlinmec.2021.103903.

[38] Habib, G., Cirillo, G.I., Kerschen, G., 2017. Uncovering detached resonance curves in single-degree-of-freedom systems. Procedia Engineering 199, 649–656. doi:https://doi.org/10.1016/j.proeng.2017.09.116. x International Conference on Structural Dynamics, EURODYN 2017.

[39] Habib, G., Cirillo, G.I., Kerschen, G., 2018. Isolated resonances and nonlinear damping. Nonlinear Dynamics 93, 979–994. doi:10.1007/s11071-018-4240-z.

[40] Heinze, T., Panning-von Scheidt, L., Wallaschek, J., 2020. Global detection of detached periodic solution branches of friction-damped mechanical systems. Nonlinear Dynamics 99, 1841–1870. doi:10.1007/s11071-019-05425-4.

[41] Hill, T., Cammarano, A., Neild, S., Wagg, D., 2015. Interpreting the forced responses of a two-degree-of-freedom nonlinear oscillator using backbone curves. Journal of Sound and Vibration 349, 276–288. URL: https://www.sciencedirect.com/science/article/pii/S0022460X15002485, doi:https://doi.org/10.1016/j.jsv.2015.03.030.

[42] Hill, T., Neild, S., Cammarano, A., 2016. An analytical approach for detecting isolated periodic solution branches in weakly nonlinear structures. Journal of Sound and Vibration 379, 150–165. doi:https://doi.org/10.1016/j.jsv.2016.05.030.

[43] Hong, D., Hill, T.L., Neild, S.A., 2019. Conditions for the existence of isolated backbone curves. Proceedings of the Royal Society A: Mathematical, Physical and Engineering Sciences 475, 20190374. doi:10.1098/rspa.2019.0374.

[44] Janovský, V., Plecháč, P., 1992. Computer–aided analysis of imperfect bifurcation diagrams, i. simple bifurcation point and isola formation centre. SIAM Journal on Numerical Analysis 29, 498–512. doi:10.1137/0729030.

[45] Jepson, A., Spence, A., 1985. Folds in solutions of two parameter systems and their calculation. part I. SIAM Journal on Numerical Analysis 22, 347–368. doi:10.1137/0722021.

[46] Jepson, A.D., Spence, A., 1989. On a Reduction Process for Nonlinear Equations. SIAM Journal on Mathematical Analysis 20, 39–56. URL: https://doi.org/10.1137/0520004, doi:10.1137/0520004. _eprint: https://doi.org/10.1137/0520004.

[47] Kay, S.R., Scott, S.K., Lignola, P.g., Gray, P., 1987. The application of singularity theory to isothermal autocatalytic reactions: the influence

of uncatalysed reactions. Proceedings of the Royal Society of London. A. Mathematical and Physical Sciences 409, 433–448. doi:10.1098/rspa.1987.0024.

[48] Kernevez, J.P., Liu, Y., Seoane, M.L., Doedel, E.J., 1990. Optimization by Continuation, in: Roose, D., Dier, B.D., Spence, A. (Eds.), Continuation and Bifurcations: Numerical Techniques and Applications. Springer Netherlands, Dordrecht, pp. 349–362. URL: https://doi.org/10.1007/978-94-009-0659-4_23, doi:10.1007/978-94-009-0659-4_23.

[49] Krack, M., Gross, J., 2019. Harmonic Balance for Nonlinear Vibration Problems. doi:https://doi.org/10.1007/978-3-030-14023-6.

[50] Kuether, R., Renson, L., Detroux, T., Grappasonni, C., Kerschen, G., Allen, M., 2015. Nonlinear normal modes, modal interactions and isolated resonance curves. Journal of Sound and Vibration 351, 299–310. doi:https://doi.org/10.1016/j.jsv.2015.04.035.

[51] Lazarus, A., Thomas, O., 2010. A harmonic-based method for computing the stability of periodic solutions of dynamical systems. Comptes Rendus Mécanique 338, 510 – 517. doi:https://doi.org/10.1016/j.crme.2010.07.020.

[52] Marler, R., Arora, J., 2004. Survey of multi-objective optimization methods for engineering. Structural and Multidisciplinary Optimization 26, 369–395. URL: https://doi.org/10.1007/s00158-003-0368-6, doi:10.1007/s00158-003-0368-6.

[53] Martinovich, K., Kiss, A.K., 2023. Nonlinear effects of saturation in the car-following model. Nonlinear Dynamics 111, 2555–2569. URL: https://doi.org/10.1007/s11071-022-07951-0, doi:10.1007/s11071-022-07951-0.

[54] Moore, G., Spence, A., 1980. The calculation of turning points of nonlinear equations. SIAM Journal on Numerical Analysis 17, 567–576.

[55] Mélot, A., Denimal, E., Renson, L., 2024. Multi-parametric optimization for controlling bifurcation structures. Proceedings of the Royal Society A: Mathematical, Physical and Engineering Sciences doi:10.1098/rspa.2023-0505.

[56] Mélot, A., Rigaud, E., Perret-Liaudet, J., 2022. Bifurcation tracking of geared systems with parameter-dependent internal excitation. Nonlinear Dynamics 107, 413–431. URL: https://doi.org/10.1007/s11071-021-07018-6, doi:10.1007/s11071-021-07018-6.

[57] Mélot, A., Rigaud, E., Perret-Liaudet, J., 2023. Robust design of vibro-impacting geared systems with uncertain tooth profile modifications via bifurcation tracking. International Journal of Non-Linear Mechanics 149, 104336. URL: https://www.sciencedirect.com/science/article/pii/S0020746222003067, doi:https://doi.org/10.1016/j.ijnonlinmec.2022.104336.

[58] Nguyen, D.H., Hill, T.L., Lowenberg, M.H., 2023. Isola in a linear one-degree-of-freedom feedback system with actuator rate saturation. International Journal of Mechanical System Dynamics , 1–6doi:https://doi.org/10.1002/msd2.12079.

[59] Nguyen, D.H., Lowenberg, M.H., Neild, S.A., 2021. Frequency-domain bifurcation analysis of a nonlinear flight dynamics model. Journal of Guidance, Control, and Dynamics 44, 138–150. doi:10.2514/1.G005197.

[60] Pedersen, N., 2005. Designing plates for minimum internal resonances. Structural and Multidisciplinary Optimization 30, 297–307. URL: https://doi.org/10.1007/s00158-005-0529-x, doi:10.1007/s00158-005-0529-x.

[61] Peeters, M., Viguié, R., Sérandour, G., Kerschen, G., Golinval, J.C., 2009. Nonlinear normal modes, part ii: Toward a practical computation using numerical continuation techniques. Mechanical Systems and Signal Processing 23, 195–216. URL: https://www.sciencedirect.com/science/article/pii/S0888327008001027, doi:https://doi.org/10.1016/j.ymssp.2008.04.003. special Issue: Non-linear Structural Dynamics.

[62] Perret-Liaudet, J., Rigaud, E., 2006. Response of an impacting hertzian contact to an order-2 subharmonic excitation : Theory and experiments. Journal of Sound and Vibration 296, 319–333. URL: https://www.sciencedirect.com/science/article/pii/S0022460X06002288, doi:https://doi.org/10.1016/j.jsv.2006.03.004.

[63] Ponsioen, S., Pedergnana, T., Haller, G., 2019. Analytic prediction of isolated forced response curves from spectral submanifolds. Nonlinear Dynamics 98, 2755–2773. doi:10.1007/s11071-019-05023-4.

[64] Renson, L., Shaw, A., Barton, D., Neild, S., 2019. Application of control-based continuation to a nonlinear structure with harmonically coupled modes. Mechanical Systems and Signal Processing 120, 449–464. URL: https://www.sciencedirect.com/science/article/pii/S0888327018306691, doi:https://doi.org/10.1016/j.ymssp.2018.10.008.

[65] Rheinboldt, W.C., 1982. Computation of critical boundaries on equilibrium manifolds. SIAM Journal on Numerical Analysis 19, 653–669. doi:10.1137/0719046.

[66] Salles, L., Staples, B., Hoffmann, N., Schwingshackl, C., 2016. Continuation techniques for analysis of whole aeroengine dynamics with imperfect bifurcations and isolated solutions. Nonlinear Dynamics 86, 1897–1911. doi:https://doi.org/10.1007/s11071-016-3003-y.

[67] Saunders, B., Kuether, R., Vasconcellos, R., Abdelkefi, A., 2024. Nonlinear analysis and vibro-impact characteristics of a shaft-bearing assembly. International Journal of Non-Linear Mechanics 159, 104618. doi:https://doi.org/10.1016/j.ijnonlinmec.2023.104618.

[68] Seydel, R., 2010. Practical Bifurcation and Stability Analysis. Springer-Verlag New York. doi:https://doi.org/10.1007/978-1-4419-1740-9.

[69] Shaw, A., Hill, T., Neild, S., Friswell, M., 2016. Periodic responses of a structure with 3:1 internal resonance. Mechanical Systems and Signal Processing 81, 19–34. URL: https://www.sciencedirect.com/science/article/pii/S088832701630005X, doi:https://doi.org/10.1016/j.ymssp.2016.03.008.

[70] Spence, A., Jepson, A.D., 1984. The Numerical Calculation of Cusps, Bifurcation Points and Isola Formation Points in Two Parameter Problems. Birkhäuser Basel, Basel. pp. 502–514. doi:10.1007/978-3-0348-6256-1_35.

[71] Spence, A., Werner, B., 1982. Non-simple turning points and cusps. IMA Journal of Numerical Analysis 2, 413–427. doi:10.1093/imanum/2.4.413.

[72] Steven G. Johnson, . The NLopt nonlinear-optimization package. http://github.com/stevengj/nlopt.

[73] Szep, G., Dalchau, N., Csikasz-Nagy, A., 2021. Parameter inference with bifurcation diagrams URL: https://arxiv.org/abs/2106.04243, doi:10.48550/ARXIV.2106.04243. preprint.

[74] Thouverez, F., 2003. Presentation of the ECL benchmark. Mechanical Systems and Signal Processing 17, 195–202. URL: https://www.sciencedirect.com/science/article/pii/S0888327002915608, doi:https://doi.org/10.1006/mssp.2002.1560.

[75] Urabe, M., 1965. Galerkin's procedure for nonlinear periodic systems. Archive for Rational Mechanics and Analysis 20, 120–152. URL: https://doi.org/10.1007/BF00284614, doi:10.1007/BF00284614.

[76] Vadcard, T., Colaïtis, Y., Batailly, A., Thouverez, F., 2022. Assessment of Two Harmonic Balance Method-Based Numerical Strategies for Blade-Tip/Casing Interactions: Application to NASA Rotor 67. Journal of Engineering for Gas Turbines and Power 144, 121004. URL: https://doi.org/10.1115/1.4055416, doi:10.1115/1.4055416.

[77] Vadcard, T., Thouverez, F., Batailly, A., 2024. On the detection of nonlinear normal mode-related isolated branches of periodic solutions for high-dimensional nonlinear mechanical systems with frictionless contact interfaces. Computer Methods in Applied Mechanics and Engineering 419, 116641. doi:https://doi.org/10.1016/j.cma.2023.116641.

[78] Xie, L., Baguet, S., Prabel, B., Dufour, R., 2017. Bifurcation tracking by harmonic balance method for performance tuning of nonlinear dynamical systems. Mechanical Systems and Signal Processing 88, 445–461. doi:https://doi.org/10.1016/j.ymssp.2016.09.037.